JCI insight

Insights into *KIF11* pathogenesis in Microcephaly-Lymphedema-Chorioretinopathy syndrome from a lymphatic perspective

Kazim Ogmen, Sara E. Dobbins, Rose Yinghan Behncke, Ines Martinez-Corral, Ryan C.S. Brown, Michelle Meier, Sascha Ulferts, Nils Rouven Hansmeier, Ege Sackey, Ahlam Alqahtani, Christina Karapouliou, Dionysios Grigoriadis, Juan C. Del Rey Jimenez, Michael Oberlin, Denise Williams, Arzu Ekici, Kadri Karaer, Steve Jeffery, Peter Mortimer, Kristiana Gordon, Kazuhide S. Okuda, Benjamin M. Hogan, Taija Mäkinen, René Hägerling, Sahar Mansour, Silvia Martin-Almedina, Pia Ostergaard

JCI Insight. 2025. https://doi.org/10.1172/jci.insight.177656.

Research In-Press Preview **Clinical Research** **Genetics** **Vascular biology**

Pathogenic variants in kinesin *KIF11* underlie microcephaly-lymphedema-chorioretinopathy (MLC) syndrome. Although well known for regulating spindle dynamics ensuring successful cell division, the association of *KIF11* (encoding EG5) with development of the lymphatic system, and how *KIF11* pathogenic variants lead to lymphatic dysfunction and lymphedema remain unknown. Using patient-derived lymphoblastoid cells, we demonstrated that MLC patients carrying pathogenic stop-gain variants in *KIF11* have reduced mRNA and protein levels. Lymphoscintigraphy showed reduced tracer absorption, and intestinal lymphangiectasia was detected in one patient, pointing to impairment of lymphatic function caused by *KIF11* haploinsufficiency. We revealed that KIF11 is expressed in early human and mouse development with the lymphatic markers VEGFR3, Podoplanin and PROX1. In zebrafish, scRNA-seq identified *kif11* specifically expressed in endothelial precursors. In human lymphatic endothelial cells (LECs), EG5 inhibition with Ispinesib, reduced VEGFC-driven AKT phosphorylation, migration and spheroid sprouting. *KIF11* knockdown reduced *PROX1* and *VEGFR3* expression, providing for the first time a link between *KIF11* and drivers of lymphangiogenesis and lymphatic identity.

Insights into *KIF11* pathogenesis in Microcephaly-Lymphedema-Chorioretinopathy syndrome from a lymphatic perspective.

Kazim Ogmen[1], Sara E. Dobbins[1], Rose Yinghan Behncke[2,3], Ines Martinez-Corral[4#], Ryan C.S. Brown[5], Michelle Meier[5, 6, 7], Sascha Ulferts[2], Nils Rouven Hansmeier[2,8], Ege Sackey[1,9], Ahlam Alqahtani[10], Christina Karapouliou[1§], Dionysios Grigoriadis[1], Juan C. Del Rey Jimenez[9], Michael Oberlin[11], Denise Williams[12], Arzu Ekici[13], Kadri Karaer[14], Steve Jeffery[1], Peter Mortimer[1,15], Kristiana Gordon[1,15], Kazuhide S. Okuda[5,6‡], Benjamin M. Hogan[5,6], Taija Mäkinen[4,16,17], René Hägerling[2,3,8], Sahar Mansour[1,9*], Silvia Martin-Almedina[1*], Pia Ostergaard[1]

[1] School of Health & Medical Sciences, City St George's, University of London, London SW17 0RE, UK.
[2] Research Group 'Lymphovascular Medicine and Translational 3D-Histopathology', Institute of Medical and Human Genetics, Charité - Universitätsmedizin Berlin, Germany.
[3] Berlin Institute of Health at Charité - Universitätsmedizin Berlin, BIH Center for Regenerative Therapies, Berlin, Germany.
[4] Department of Immunology, Genetics and Pathology, Uppsala University, Sweden.
[5] Organogenesis and Cancer Program, Peter MacCallum Cancer Centre, Melbourne, Victoria, Australia.
[6] Sir Peter MacCallum Department of Oncology and Department of Anatomy and Physiology, University of Melbourne, Australia.
[7] Bioinformatics Core Facility, Peter MacCallum Cancer Centre, Melbourne, Victoria, Australia.
[8] Research Group Development and Disease, Max Planck Institute for Molecular Genetics, Berlin, Germany.
[9] South West Thames Centre for Genomics, St George's University Hospitals NHS Foundation Trust, London, UK.
[10] Bioscience Institute, Wolfson Childhood Cancer Research Centre, Brewery Lane, Newcastle University, Newcastle upon Tyne, NE1 7RU, UK.
[11] Földiklinik GmbH & Co. KG, European Center for Lymphology Black Forest, Hinterzarten, Germany.
[12] The National Congenital Anomaly and Rare Diseases Registration Services (NCARDRS) NHS England, The Birmingham Government Hub, Birmingham, B2 4BH.
[13] University of Health Sciences, Bursa Yüksek İhtisas Training and Research Hospital, Department of Pediatric Neurology, Bursa, Turkey.

[14] Department of Medical Genetics, Pamukkale University Faculty of Medicine, Denizli, Turkiye.
[15] Dermatology & Lymphovascular Medicine, St George's University Hospitals NHS Foundation Trust, London, UK.
[16] Translational Cancer Medicine Program and Department of Biochemistry and Developmental Biology, University of Helsinki, Haartmaninkatu 8, 00014 Helsinki, Finland.
[17] Wihuri Research Institute, Haartmaninkatu 8, 00290 Helsinki, Finland.

[#] Current affiliation: Univ. Lille, Inserm, CHU Lille, Laboratory of Lille Neuroendocrinology, Lille Neuroscience & Cognition, UMR-S1172, EGID, DISTALZ, F- 59000 Lille, France.
[§] Current affiliation: Developmental Biology and Cancer Department, Great Ormond Street Institute of Child Health, University College London, London, UK.
[‡] Current affiliation: Centre for Cardiovascular Biology and Disease Research, La Trobe Institute for Molecular Science, Department of Biochemistry and Chemistry, School of Agriculture, Biomedicine and Environment, La Trobe University, Australia.
[*] Clinical correspondence to Sahar Mansour, South West Thames Centre for Genomics, City St George's University of London, Cranmer Terrace, London SW17 0RE, United Kingdom. E-mail: smansour@citystgeorges.ac.uk. Phone number: 020 8725 0569. ORCID: 0000-0001-6629-4118. Research-related correspondence to Silvia Martin-Almedina, School of Health and Medical Sciences, City St George's University of London, Cranmer Terrace, London SW17 0RE, UK. E-mail: smartina@citystgeorges.ac.uk. Phone number: 020 8725 3623. ORCID: 0000-0001-5282-6662.

Conflict-of-interest statement

The authors have declared that no conflict of interest exists.

Abstract

Pathogenic variants in kinesin *KIF11* underlie microcephaly-lymphedema-chorioretinopathy (MLC) syndrome. Although well known for regulating spindle dynamics ensuring successful cell division, the association of *KIF11* (encoding EG5) with development of the lymphatic system, and how *KIF11* pathogenic variants lead to lymphatic dysfunction and lymphedema remain unknown.

Using patient-derived lymphoblastoid cells, we demonstrated that MLC patients carrying pathogenic stop-gain variants in *KIF11* have reduced mRNA and protein levels. Lymphoscintigraphy showed reduced tracer absorption, and intestinal lymphangiectasia was detected in one patient, pointing to impairment of lymphatic function caused by *KIF11* haploinsufficiency.

We revealed that *KIF11* is expressed in early human and mouse development with the lymphatic markers VEGFR3, Podoplanin and PROX1. In zebrafish, scRNA-seq identified *kif11* specifically expressed in endothelial precursors. In human lymphatic endothelial cells (LECs), EG5 inhibition with Ispinesib, reduced VEGFC-driven AKT phosphorylation, migration and spheroid sprouting. *KIF11* knockdown reduced *PROX1* and *VEGFR3* expression, providing for the first time a link between *KIF11* and drivers of lymphangiogenesis and lymphatic identity.

Introduction

Microcephaly-lymphedema-chorioretinopathy syndrome (MLC; ORPHA:2526), also known as 'microcephaly with or without chorioretinopathy, lymphedema, or intellectual disability' syndrome, is an autosomal dominant condition with about 50% of patients presenting with congenital primary lymphedema (1). Variants in *KIF11* cause 75% of MLC cases (1-3). The pathogenic basis of *KIF11*-associated retinal vascular disease has been investigated through the generation of a mouse model for familial exudative vitreoretinopathy (FEVR) (4). More recently, the phenotypic spectrum of *KIF11*-associated MLC has been expanded to include renal system involvement (5). However, how *KIF11* variants lead to lymphedema, the specific hallmark of lymphatic dysfunction, is not known.

KIF11 encodes EG5, a motor protein essential in cell cycle dynamics. EG5 inhibition arrests cells in metaphase inducing monopolar spindles in vitro (6, 7). No phenotype was found in heterozygous mice ($Eg5^{+/-}$), but homozygous deletion ($Eg5^{-/-}$) was lethal in the embryo (8, 9).

Recently, several groups found roles for EG5 independent of cell division, e.g. cell migration, intracellular vesicle trafficking or regulation of primary cilia dynamics in several cell models including post-mitotic neurons (10-15). These studies could explain the pleiotropic and variable phenotype characteristic of MLC syndrome, potentially related to the diverse functions of EG5, which may even be cell type dependent.

Here we investigate the clinical features and disease mechanisms in MLC patients with *KIF11* pathogenic variants, focusing on lymphatic function. They typically presented with congenital onset lower limb lymphedema, mostly in the dorsum of the foot. Clinically their phenotype resembles that of Milroy disease and lymphoscintigraphy scans showed functional aplasia. Significant issues with intestinal lymphangiectasia were noted in one of the individuals, which has been only reported once in MLC patients (16), but is characteristic of other primary lymphatic anomalies (17, 18).

We hypothesise that there is a critical role for *KIF11* (EG5) in the lymphatics, possibly through interactions with VEGFR3. We show that *KIF11* co-expresses with *VEGFR3* in the initial steps of lymphangiogenesis in early human and mouse embryonic development. In zebrafish *kif11* expression is associated with proliferation of endothelial progenitors. In vitro loss-of-function models show that *KIF11* inactivation decreases proliferation, migration and sprouting after VEGFC treatment of serum-starved human dermal lymphatic endothelial cells (LECs). Here we provide first insights into the association of EG5 with lymphatic development and function in health and disease. More research into the specific roles of EG5 at defined lymphatic developmental stages is required to characterise disease mechanisms and delineate target treatments for MLC patients.

Results

MLC patients show lymphatic functional defects.

Lymphedema in MLC patients is mostly bilateral, affecting lower limbs (Figure 1A) (1, 3). We evaluated ten patients with an MLC phenotype, six individuals from four families carrying two different unreported *KIF11* variants: c.2680C>T; p.(Q894*) and c.2922G>A; p.(P974=), and four individuals from two previously reported families (3) carrying pathogenic variants in *KIF11,* c.1159C>T; p.(R387*) and c.1039_1040delCT; p.(L347Efs*8). Clinical summaries are in Supplemental Table 1 and Supplemental Table 2, and variant summaries in Supplemental Table 3. Pedigrees are shown in Supplemental Figure 1.

Lymphatic function of the lower limbs was assessed in three individuals using lymphoscintigraphy. Quantification of the tracer signal 2 hours post injection revealed that almost 100% of activity was retained in the feet of the most affected limbs with a reduced uptake in the groin of 0.1-0.4% (Table 1). Proband F1-II.1, who presented with congenital bilateral lymphedema, showed absence of radioactive isotope uptake from the web spaces between the toes (i.e. functional aplasia) as described previously (3) (Figure 1B). Two siblings, F3-II.1 and F3-II.2, presenting with microcephaly and congenital bilateral lower limb lymphedema (Figure 1A) also demonstrated abnormalities on their lymphoscintigraphy images (Figure 1, C-D). One leg is more affected than the other in both siblings, but with evidence of functional aplasia in one leg the findings are in keeping with an underlying bilateral primary lymphedema compared to the control (Figure 1E, a historical standard from authors' archive).

Proband F4-II.1 presented with dysphagia, intermittent diarrhoea, and failure to thrive; a clinical observation not typical of MLC. Podoplanin staining of intestinal biopsies showed dilated lymph vessels (lacteals) in the duodenum (Figure 1F), and together with the significantly increased Alpha 1 antitrypsin (A1AT)-values in the stool, is consistent with protein-losing enteropathy (PLE) caused by intestinal lymphangiectasia. Immunofluorescence staining revealed reduced lymphatic vessel density compared to healthy control samples based on Podoplanin positive area per tissue area (Figure 1G).

MLC patients show reduced expression of KIF11 (EG5) pointing to haploinsufficiency as the disease mechanism.

To ascertain the disease mechanism in MLC, we analysed the expression of *KIF11* in lymphoblastoid cell lines, blood and saliva from four patients carrying pathogenic variants (leading to a premature termination) in the motor domain (L347Efs*8) and the coiled-coil domain 1 (R387*) (Figure 2A). These regions are involved in protein oligomerisation (19) and vesicle tethering (20), respectively, and thus seem likely that both variants will negatively

impact on EG5 function. qRT-PCR analysis of blood (Figure 2B) and saliva (data not shown) using allele-specific primers for the wild-type (wt) allele and each of the mutant alleles (mut) showed strong reduction, but not a complete absence of the mutant mRNA in all samples. This fits with nonsense mediated RNA decay, and the then expected level of wt *KIF11* mRNA of 50% in patients' samples compared to the controls. Western blot analysis of protein lysates from lymphoblastoid cell lines also showed around 50% levels of EG5 protein compared to the controls (Figure 2C). Interestingly, a truncated protein of expected size (43KDa) was detected in F1-II.1 (Figure 2D).

A synonymous variant in KIF11 causes cryptic splicing which leads to exon skipping.

Three MLC patients in this study carry the same synonymous variant c.2922G>A; p.(P974=) (Supplemental Table 1) and *in silico* prediction tools suggest the variant is pathogenic (Supplemental Table 3). RNA was isolated from patient F5-II.1, converted into cDNA and Sanger sequenced. The synonymous variant causes cryptic splicing which leads to the removal of a 108bp fragment of exon 20 (r.2815_2922del) (Figure 2E) possibly leading to a shortened EG5 protein (p.V939_P974del) lacking part of the BimC-box tail domain. This C-terminal domain appears to be a crucial region in microtubule binding and a previously described pathogenic variant (p.R944C) in this region has been reported (3)**.**

KIF11 co-expresses with lymphatic VEGFR3 positive structures during human embryonic development.

In silico analyses show kinesin transcripts, including *KIF11*, are enriched in the endothelial expressed sequence tag (EST) pool (21), and human foreskin sections showed positive co-staining of EG5 with CD31 and Podoplanin, confirming the expression of EG5 in adult lymphatics. As MLC is characterised by early onset lymphedema there is a need to understand *KIF11* expression patterns during lymphatic embryonic development. Human embryonic tissues at different developmental stages ranging from human Carnegie stage 12 (CS12) to CS22 were analysed for *KIF11* mRNA expression along with different lymphatic specific markers (*VEGFR3* and *PROX1* or *PDPN*) using RNA-scope multiplexing *in-situ* hybridization. Although co-expression of *KIF11*, *PROX1* and *VEGFR3* was found in the hepatic primordia (HP), little or no co-expression of *KIF11* with other lymphatic markers was seen around the developing cardinal vein (CV) at CS12 (Figure 3A). Later at CS15, low expression levels of *KIF11,* with co-expression to *PROX1* and *VEGFR3,* was detected around the CV. At CS18, increased expression of *KIF11* with *VEGFR3* and *PDPN* positive cells was found around the CV. These VEGFR3 positive cells would migrate from the cardinal vein to form the primordial thoracic duct (pTD), formerly known as the lymphatic sacs (22). Later in development, at CS22, the association between *KIF11* and lymphatic markers was maintained as the lymphatic

vessel network expanded. This indicates that *KIF11* is associated with the development of lymphatic vessels at the later stages analysed.

KIF11 expression might be regulated by lymphatic transcription factors in human lymphatic endothelial cells.

To understand the relationship between *KIF11* expression and key transcriptional regulators of lymphatic development, we analysed publicly available ChIP-seq data of primary human dermal LECs (23) to identify regions on *KIF11* bound by GATA2, FOXC2, NFATC1 and PROX1. We identified binding of FOXC2 and NFATC1 in intron 17 (chromosomal position chr10:92,640,060-92,640,600) and binding of PROX1 approximately 1.3kb upstream of the *KIF11* promoter (chr10:92,591,500-92,592,000) (Figure 3B)**.** Both peaks overlap with ENCODE enhancer-like signals predicted from DNase hypersensitivity, histone modification or CT-CF binding, with data combined across cell types (24). To experimentally confirm that PROX1 and FOXC2 may regulate *KIF11* expression, LECs were treated with either siRNA *PROX1* or siRNA *FOXC2* and *KIF11* expression evaluated by RT-qPCR, showing downregulation (Figure 3C).

Kif11 co-expresses with lymphatic Flt4-positive structures during mouse embryonic development and in adult mouse intestine.

In mice, lymphatic vessels develop at around developmental day E10.0. A subpopulation of PROX1-positive cells, so called initial LECs (iLECs), leave the cardinal vein (CV) and form the primordial thoracic duct (pTD) (22). A second lumenized lymphatic vessel, the peripheral longitudinal lymphatic vessel (PLLV) is formed simultaneously, which represents a potential source or vascular connection site for dermal lymphatic vessels (22). We therefore investigated the expression of *Kif11* and *Flt4* in the CV, iLECs, the pTD and dermal LECs/PLLVs.

First, we located the relevant lymphatic structures by H&E staining (Figure 4A [A, F, K, P]) and immunofluorescence (Figure 4A [B, G, L, Q]) on mouse embryonic slides from E10.5 to E13.5. Using RNAscope, we identified a very weak *Flt4* mRNA signal in the CV (Figure 4A [EA and ED]), but robust *Flt4*mRNA signal in iLECs (Figure 4A [DA and DD]) at E10.5. From E11.5-E13.5 when the formation of the pTD/lymph sac begins, there is an increased intensity of expression of *Flt4* in the cells lining the structure (Figure 4A [JA and JD, OA and OD, TA and TD]). This increase of signal in developing and expanding lymphatic vessels is consistent with the finding in humans at later developmental stages (e.g. CS22, Figure 3A).

Kif11 mRNA signal was detected to co-express with cells expressing *Flt4* from E11.5 to E13.5 in the pTD (Figure 4A [JA and JC, OA and OC, TA and TC]) at relatively constant levels albeit of a lower signal intensity (Figure 4B). Likewise, dermal cells with a *Flt4*-positve mRNA signal

express *Kif11* (Figure 4A [IA and IC, NA and NC, SA and SC]). The *Kif11* mRNA signal appears to be 3- to 5-fold higher in dermal LECs compared to that of the pTD (Figure 4C).

We next performed immunofluorescence staining with an anti-EG5 antibody, anti-VEGFR3 antibody and anti-Ki67 antibody to also assess proliferation in E10.5 and E12.5 mouse embryonic slides (Figure 5). As we had observed using RNAscope, we saw a protein co-expression pattern of EG5 and VEGFR3 that mirrors the previously detected mRNA co-expression. EG5 protein co-localizes with VEGFR3-positive cells in the primitive thoracic duct (pTD) at both E10.5 and E12.5 stages, though the EG5 signal appeared consistently lower in intensity (Figure 5, CC-CD and FC-FD). Similarly, dermal VEGFR3-positive cells also expressed EG5, with stronger EG5 signal intensity in dermal LECs compared to those in the pTD (Figure 5, BC-BD and EC-ED). Co-staining for EG5, Ki67 and VEGFR3 reveals only limited overlap, indicating a low proliferative rate during early lymphatic vessel development in the mouse at the investigated developmental stages (Figure 5, BB-BC-BD and EB-EC-ED).

Due to the phenotype observed in MLC patients we performed whole-mount immunofluorescence staining in adult ear and intestinal mouse tissues isolated from 2 months old mice. In the adult mouse intestine, we detected robust protein co-expression of EG5 and VEGFR3 in the lacteals (Figure 5, HA-HC-HD and IA-IC-ID). In contrast, no detectable EG5 protein signal is observed in the adult mouse ear (Figure 5, KA-KC-KD and LA-LC-LD).

To complement our mouse development investigations, we interrogated publicly available scRNA-seq datasets (25, 26). Analysis of single cell transcriptomics data of healthy mouse skin tissue demonstrates *Kif11* expression is detected in proliferative LECs with significantly increased proportion of cells expressing *Kif11* compared to other cell types (pairwise chi-sq $P< 0.001$, Supplemental Figure 2, A-B). This effect is also seen in an additional single cell LEC transcriptomics dataset (Supplemental Figure 2, C-D).

kif11 expression is associated with highly proliferative lymphatic and blood endothelial precursors during zebrafish embryonic development.

To model the pathogenic basis of *KIF11*-associated disease, we used CRISPR-Cas9 to generate a zebrafish *kif11* mutant model harbouring an 8bp deletion within the coding sequence (Supplemental Figure 3A). This allele was designated *kif11*^{uom131}. Similar to a number of previously reported pathogenic *KIF11* variants (3, 16), the deletion induces a frameshift and subsequent stop codon, predicted to truncate the kinesin motor domain of Eg5 (Supplemental Figure 3A). Analysis of sibling (*kif11*$^{+/+\ or\ +/uom131}$) and *kif11*^{uom131} homozygous mutants revealed a developmental phenotype at 14 and 17 hpf (hours post fertilisation). Mutant embryos displayed abnormal development of the brain and showed somitogenesis defects, as well as a delay in embryonic development based on somite

numbers (Figure 6A). At 24hpf, homozygous mutant embryos showed brain necrosis, abnormal eye development and delayed embryonic development, including the formation of vasculature (Figure 6B). Homozygous embryos also had no circulation at 28 hpf or 48 hpf (n=33/111 at 28 hpf, n=11/56 at 48 hpf) (data not shown). This led to embryonic lethality by 2-3 days post fertilisation (dpf), which precluded the analysis of the lymphatic lineage. Heterozygous mutants were indistinguishable from wildtype including in lymphatic development (Supplemental Figure 3B). These defects are consistent with aspects of the human phenotype but could be considered more severe than the human phenotypes reported to date (1, 16).

To further explore the impact of *kif11*/Eg5 loss-of-function in zebrafish, we next treated embryos with carefully optimised concentrations of the Eg5 inhibitor Ispinesib (Supplemental Figure 3C). To avoid severe early developmental phenotypes, we treated at stages following embryonic gastrulation. Treatment from 10 hpf led to a partial phenocopy of the mutant phenotype described above with brain necrosis and tail extension defects (Figure 6C), suggesting that the inhibitor is likely generating a loss-of-function model. Next, we treated embryos with 50μM Ispinesib from 24 hpf and analysed them at 72hpf to allow normal vasculogenesis and angiogenesis to occur before assessing *kif11*/Eg5 function in vasculature. Treatment at this stage generated embryos that developed normal blood circulation and major vascular lineages such as the DA, PCV and ISVs, however we observed reductions in the total number of LECs and dorsal aorta endothelial cells (Figure 6D, E, F). Together this suggests that *kif11*/Eg5 has a broad function in embryonic development and is important for the normal development of vasculature in the embryo.

To gain further insight into the role of *kif11*, we analysed recently published scRNA-seq data of wildtype zebrafish populations at 3 and 4dpf (27). *kif11* expression was evaluated across all reported cell types (Supplemental Figure 3, D and F) and compared to proliferation markers, *pcna* and *mki67*. *kif11* expression was positively correlated with the expression of proliferation markers *mki67* and *pcna* (Supplemental Figure 3, E and G). This suggests a role in highly proliferating EC populations that would include LECs of the developing embryo and is in line with the suggested role of this protein in cytokinesis (28).

KIF11 inhibition impairs VEGFC driven cell migration and sprouting in LECs.

VEGFR3 is the essential signalling protein in maintaining lymphatic function. The similarities between the congenital bilateral lower limb lymphedema and functional aplasia on lymphoscintigraphy imaging seen in Milroy disease (caused by pathogenic *VEGFR3* variants) and MLC (caused by pathogenic *KIF11* variants), and the co-expression of *KIF11* and

VEGFR3 during human and mouse embryonic development, may suggest a common functional pathway.

With *KIF11* haploinsufficiency confirmed as the disease mechanism, we generated two loss-of-function approaches to block EG5 function: siRNA transfection and a specific EG5 antagonist, Ispinesib, widely used to investigate EG5 function in several cell models including HUVEC (21). After 24h, siRNA *KIF11* transfection in LECs reduced >80% EG5 protein expression (Supplemental Figure 4A) with the expected decrease in cell proliferation measured as %EdU^{+} LECs (Supplemental Figure 4B). Spindle pole formation after Ispinesib treatment (0.5nM-50nM) was evaluated by α tubulin staining (Supplemental Figure 4D). Ispinesib at 5nM-50nM caused an abnormal distribution of the filament fibers, compared to vehicle treated cells, due to the inhibition of the kinesin motor function necessary for the assembly of the microtubules (29), verifying the inhibitory effect of Ispinesib on mitotic function of EG5 at the analyzed doses. Toxicity was tested in a spheroid-based assay by measuring fluorescence uptake of a dye by viable cells. 50-100nM Ispinesib treated spheroids showed comparable fluorescence levels to DMSO controls and retained some ability to sprout, whereas 200nM treated spheroids showed increased toxicity as well as impaired sprouting ability (Supplemental Figure 4E).

To investigate the possible role of EG5 in regulating LEC migration, firstly, we performed in vitro transwell migration assays to measure the ability of LECs to migrate towards VEGFC. Ispinesib inhibited migration in a dose-dependent manner and a 50% reduction was seen after 50nM Ispinesib treatment (Figure 7A). With an approximately 50% loss of *KIF11* expression in MLC patients (Figure 2, B-C), we sought to use 50nM Ispinesib for further experiments as our haploinsufficiency in vitro model.

To further analyze migration parameters in more detail, we performed wound healing experiments tracking single cells moving into the wound. The aim was to study the role of EG5 on cellular migration minimizing interference from cell division, considering that the average full cell cycle length of primary LECs is >20 hours. The wound was fully closed after 15 hours in the control condition, but a delay was observed in 50nM Ispinesib treated cells (Figure 7B, Supplemental Video 1) as well as a reduction of the number of cells in the experimental wound window over time (Figure 7C). Star plots showed different direction migration patterns between control and Ispinesib treatments (Figure 7D), and velocity analysis indicated a significant reduction of individual cell speed in Ispinesib treated cells with the mean velocity of cells at 2.08 for control vs 1.94 for 50nM Ispinesib treated cells (Wilcoxon-rank-sum test; p-value<$2.2x10^{-16}$).

Lymphatic sprouting is a key process driving lymphangiogenesis in the developing lymphatic system, which requires collective action of both proliferation of stalk and migration of tip cells (30). We assessed the role of EG5 in LEC sprouting using an in vitro 3D spheroid assay. After 24h, 150ng/mL VEGFC increased the average sprouting length by 60%, and the number of sprouts by 30%, per spheroid compared to the vehicle control. This was reduced in a dose-dependent manner by Ispinesib treatment (Figure 7E). 50nM Ispinesib caused approximately 50% reduction on both the average length and the number of sprouts compared to VEGFC only, and 100nM Ispinesib completely abolished VEGFC-induced sprouting. Overall, the data suggests a role for EG5 in LEC sprouting, probably due to a combination of both the impact on proliferation and migration. To differentially test the effects purely on migration, we attempted to inhibit proliferation prior to Ispinesib treatment, however in our hands, the combination of Ispinesib and aphidicolin (a cell cycle inhibitor) was very damaging for the cells (data not shown).

KIF11 inhibition reduces VEGFC-induced VEGFR3 signalling leading to loss of AKT and MAPK phosphorylation.

To understand the impact of *KIF11* haploinsuficiency on lymphatic endothelial cell signalling pathways regulating migration and sprouting we used Proteome Profiles Human Phospho-Kinase Array (R&D) to detect phosphorylation changes in 43 human kinases in siRNA *KIF11* treated LECs compared to siRNA control. Quantification of the signal intensities demonstrated no striking changes in phosphorylation patterns, but we could detect decreased phosphorylation of p38MAPK and AKT1 (at both positions Ser-473 and Thr-308), and an increase in phosporylation of other kinases including JUN and TP53 (Figure 8A), the last associated with spindle defects and stress response (31). We explored the molecular interactions derived from the human phospho-kinase analysis, plus the already known interactions described in the literature and public databases, by pathway analysis using STRING and Cytoscape. A selection of the kinase networks generated, showing interactions and the direction of the phophorylation changes (blue, decrease of phosporylation; red, increase of phosphorylation) are shown in Figure 8B.

We focused our attention on the AKT and MAPK signalling pathways, that appeared downregulated after siRNA *KIF11* treatment, and are two of the major downstream effectors of tyrosine kinase receptor signalling including VEGFR3. LECs were pretreated overnight with DMSO (vehicle) or 50nM Ispinesib, and were stimulated the next day with 100ng/ml VEGFC for up to 45 minutes. VEGFC treatment activated the phosphorylation levels of MAPK and AKT both in DMSO and Ispinesib treated cells. Ispinesib treatment resulted in a significant reduction of MAPK phosphorylation at 10-15 min and AKT phosphorylation at 45 minutes post-VEGFC stimulation compared to DMSO treatment (Figure 8C).

KIF11 knockdown downregulated PROX1, VEGFR3 and cell junction molecule expression.
PROX1 is a master regulator of LEC specification (32) regulating genes and proteins important for maintenance of LEC identity such as VEGFR3 and Podoplanin (33, 34) and transcription factors essential for lymphatic valve morphogenesis like FOXC2 (35). To determine whether downregulation of lymphatic markers might also contribute to the lymphatic defects observed with *KIF11* haploinsufficiency, we transfected siRNA *KIF11* for 48 and 72 hours in LECs and investigated the effect on the expression of well-characterised lymphatic endothelial markers. After 48 hours we detected approximately 50% downregulation of *FLT4* (VEGFR3) gene expression and *PROX1* both at mRNA (Figure 8D) and protein (Figure 8E) levels. Other lymphatic identity markers such as *FOXC2* and *LYVE1* showed significant reduction after 72 hours whereas the gene expression of *PDPN* remained unaffected (Figure 8D). These results were confirmed with a second siRNA sequence (siRNA KIF11 #7) (Supplemental Figure 4, A and C).

Lymphoscintigraphy (Figure 1, B-D) revealed a lack of interstitial fluid uptake in MLC patients suggesting the initial lymphatic capillaries may be dysfunctional. The permeability of the lymphatic capillaries is critical for functional fluid uptake and is controlled by specialised junctions (36) and the importance of this specialized junctional organization has already been probed in several animal models (37-39). Since it is crucial to understand the role of EG5 in controlling lymphatic junction architecture and permeability, and its contribution to lymphatic (dys)function (e.g. failure of fluid uptake in lymphatic capillaries), we looked next at the impact of *KIF11* depletion on the expression of cell junction molecules and found downregulation of *TJP1* (encoding ZO-1), *CLDN5* (encoding Claudin-5) and *CDH5* (encoding VE-Cadherin) (Figure 8D and Supplemental Figure 4C).

Discussion

Autosomal dominant pathogenic variants in *KIF11* (EG5) are causative of microcephaly-lymphedema-chorioretinopathy (MLC) syndrome, a condition that presents with a variable spectrum of central nervous system, lymphatic, renal and ocular developmental anomalies (1, 5, 16). We have a better understanding of the ubiquitous functions of EG5 and its involvement in the onset and progression of several pathologies (40). Since the association of *KIF11* with MLC (3), we have aimed to understand how EG5 variants account for the lymphatic phenotype presented in this pleiotropic disease. Very little was previously understood about the underlying mechanisms leading to lymphatic failure, partly due to the limited knowledge about the role of *KIF11* in the development and maintenance of the lymphatic system. A better understanding of the signalling pathways and molecules that regulate lymphatic development and physiology in the context of *KIF11* pathogenesis is essential to enable the development of more targeted and accurate treatments for MLC patients.

In this study we were examining the disease mechanism(s) causing lymphedema in patients with pathogenic variants in *KIF11*, as well as investigating the molecular and cellular interactions by which *KIF11* may regulate lymphangiogenesis. We have attempted this through; 1) investigations on the clinical characteristics and lymphatic function of patients with MLC, by lymphocintigraphy and immunohistochemystry of intestinal biopsy; 2) the use of patient-derived cells to study the expression levels of *KIF11*; 3) the analysis of *KIF11* expression during embryonic lymphatic development both in mouse and human, and in adult mouse tissues; 4) the generation of MLC zebrafish models; and 5) an examination of the impact of *KIF11* haploinsufficency on VEGFR3 signalling and lymphatic identity using primary lymphatic endothelial cells as an in vitro model.

As previously reported, lymphedema in MLC patients is mostly bilateral, affecting the lower limbs. To determine whether the fault in the lymphatic function is at the initial lymphatic capillaries or at the collector level we performed lymphocintigraphy in three MLC patients carrying two stop-gain pathogenic variants in *KIF11*. Images showed a typical functional aplasia mechanism where the tracer (or most of it) was retained at the injection points, meaning a failure or reduction of the ability of the initial lymphatics. This pattern is similar to that observed in Milroy patients with pathogenic variants in *VEGFR3* (41) and suggests that the fault is in the initial lymphatic capillaries.

One patient presented with intestinal lymphangiectasia, and the staining of an intestinal biopsy revealed reduced Podoplanin positive lymphatic vessels. Reduced number of dermal lymphatic vessels has also been observed in skin biopsies from Milroy patients (42). Some mechanisms suggested to cause lymphangiectasia and impaired lacteal function include

defective LEC polarity, valve maldevelopment, lymphatic vasculature hyperplasia and junctional destabilization (43, 44). Due to the critical role of the lacteals in fat absorption and digestion (45) the lymphangiectasia observed is likely to explain the intestinal problems in this patient. Further analysis of several blood and lymphatic markers together with junctional proteins could reveal additionally structural and/or functional alterations. Only one case of intestinal lymphangiectasia had been observed in MLC before (16), therefore, our finding confirms that intestinal lymphangiectasia should be considered a feature of MLC, albeit not typical, and clinicians should perform investigations accordingly. This finding also provides new suggestions for the clinicians for patient care (e.g. prescription of a low-fat diet for intestinal lymphangiectasia in MLC patients).

Scientists have searched for the molecular disease mechanisms of MLC, suggesting pathogenic variants would most likely result in loss of function of *KIF11* due to nonsense-mediated mRNA decay, premature truncation of the protein or splicing abnormalities (16). In this study we looked at the impact of *KIF11* variants on mRNA and protein expression levels in lymphoblastoid transformed cells isolated from the blood of patients (together with blood and saliva samples) confirming that the two stop-codon variants investigated resulted in a reduction but not total loss of the mutated mRNA. As expected, qPCR and western blot analysis revealed an approximately 50% reduction of *KIF11* expression and in one case a shorter truncated EG5 protein was detected. A synonymous variant in *KIF11* investigated in this study caused cryptic splicing which led to exon skipping predicted to lead to a shorter EG5 protein. Others showed a similar effect for the synonymous variant c.2922G>T (46). Therefore, we conclude that *KIF11* haploinsufficiency is the likely underlying key disease mechanism in MLC.

We believe that to be able to explain the pathophysiology of MLC it is neccesary to understand the association of *KIF11* with the development of the lymphatic system, particularly since the expression pattern of *KIF11* in the lymphatics during development and adulhood has been poorly investigated. The early onset of lymphedema in MLC also suggests that the interaction has occurred early in development. We found *KIF11* expression associated with the development of lymphatic structures both in human and mouse embryos using RNA scope *in situ* hybridization. These findings were also confirmed by immunofluorescence of mouse embryos. Co-expression of *KIF11* was detected together with lymphatic endothelial markers such as PROX1, VEGFR3 or Podoplanin. Interestingly we found association of *KIF11* regulatory regions with the lymphatic transcription factors PROX1, FOXC2 and NFATC1. Another intriguing finding was to discover *Kif11* mRNA signal higher in dermal LECs compared to that of the pTD/lymph sacs, which could indicate a distinct role for *KIF11* (EG5) in discrete lymphatic vessel beds. We could speculate that the

relative prominence of *Kif11* expression in dermal LECs could relate to the functional aplasia of the initial dermal lymphatics observed in lymph scans from MLC patients. Moreover, when analysing the expression in adult mice, EG5 and VEGFR3 co-expression was detected in intestinal tissue suggesting a role for EG5 in this tissue after embryonic development, that could explain intestinal complications in MLC patients postnatally.

Heterozygous mutant mice generated with a genetrap insertion in *Eg5* appear phenotypically normal. In contrast, embryos homozygous for the *Eg5* null allele displayed signs of a proliferation defect suggesting EG5 is essential for cell division during early development (9). In another study, Chauviere and colleagues demonstrated that heterozygous mice are healthy, fertile, and show no detectable phenotype, whereas *Eg5*(-/-) embryos die during early embryogenesis (8). None of these studies attempted to look at the impact of *Kif11* deficiency in the lymphatic system.

The generation of in vivo models to further investigate *KIF11*'s role in lymphatic function has proved a difficult journey, most probably because of the critical role of EG5 in mitosis and the need for depleting *KIF11* early during embryo development to study its role in lymphatic development. Analysis of scRNA-seq data of wildtype zebrafish cell populations at different developmental stages confirmed the expression of *kif11* associated with highly proliferative lymphatic and blood endothelial precursors during zebrafish embryonic development. This could justify why we observed severe defects in cell survival and development that lead to early embryonic lethality. Therefore, even with the introduction of a deletion mimicking the variants observed in some MLC patients, we do not see a comparable phenotype in zebrafish. It is possible that *kif11* function may be compensated by another kinesin motor protein or that divergence in kinesin motor protein functions is at play in zebrafish. A second *kif11* loss-of-function zebrafish model was developed by treating the embryos with Ispinesib that caused a reduction of total number of LECs and dorsal aorta endothelial cells during the development of the vasculature. Altogether, this work demonstrates an essential role in early development for *kif11* and its requirement for embryo survival and vascular development in zebrafish.

We then turned to in vitro models to investigate the possible role of *KIF11* in lymphatic endothelial cells. We focussed on cell migration since the co-expression of *KIF11* and *VEGFR3* mRNA in the primordial lymphatic developing sacs could point to a possible participation of EG5 in the proliferative and migratory activity of the LEC precursor cells leaving the cardinal vein. Moreover, previous publications have highlighted this non-mitotic role linking EG5 with migration in several cell types (11, 47, 48). Our experiments suggest that LEC migration is affected by EG5 inhibition, which could be explained by the importance of microtubules in cell locomotion. Studies show how suppression of microtubule dynamics

restrained forward progression and impaired directionality (49) and is dependent on the right level of kinesin expression (50).

VEGFR3 is the master regulator of lymphatic function and development and we have previously shown that Milroy patients present with reduced size of lymphatic capillaries in their skin (42). We have also observed reduced Podoplanin-positive structures in the intestinal biopsy of an MLC patient. The remarkable similarities between the bilateral, congenital pedal lymphedema seen in Milroy disease (caused by pathogenic *FLT4* variants) and MLC (caused by pathogenic *KIF11* variants) point to a plausible convergence of both molecules in the same functional signalling axis. The co-expression of *KIF11*- and *FLT4*-positive vessels during human embryonic development supports this hypothesis of a common functional pathway.

We have observed a downregulation of AKT and MAPK phosphorylation after EG5 inhibition. Further research will be needed to investigate the specificity of VEGFC on the observed effect on AKT and MAPK phosphorylation after EG5 inhibition. A decrease of VEGFR3 signalling through loss of AKT activation could have a detrimental effect on the migratory behavour of LECs, as it has been shown that hyperactivation of PIK3CA confers a migratory LEC phenotype through increasing P-AKTSer473 (51). This finding opens a new avenue for future studies to investigate the role of EG5 in the PIK3/AKT pathway and the possibility of repurposing AKT activators (e.g. SC-79) as a potential treatment of MLC (52).

KIF11 knockdown downregulated *PROX1*, *VEGFR3* and cell junction gene expression. Other genes associated with primary lymphatic anomalies have been shown to regulate cellular junctions and permeability. For instance, abnormal cell junctions have been associated to RASopathy cases (53, 54) and EphrinB2/EPHB4 defective mice show impaired junctions (37) which could explain the edema observed. Interestingly, other kinesins have been shown to mediate VEGFR2 cell membrane recycling through Rab11, regulating vascular permeability (55). Analysis of skin biopsies from MLC patients could confirm junctional loss of integrity as the disease mechanism and possibly shed light on the functional aplasia observed.

In conclusion, we confirm *KIF11* haploinsufficiency in MLC patients as the disease mechanism and that EG5 could already play a role during embryonic lymphangiogenesis as its inhibition impairs lymphatic endothelial cell functions. We speculate whether the lymphatic impairment resulting in functional aplasia (and intestinal lymphangiectasia) observed in MLC patients could be a consequence of dysregulated VEGFR3 signalling. This would impact on the control of cell communication and signalling cascades orchestrating cell proliferation and migration during lymphangiogenesis. Our data provide the first insights into the study of *KIF11*(EG5) in lymphatic function, and future studies should elucidate the specific disease mechanisms

connecting *KIF11* pathogenic variants and lymphedema and the possibility of exploring AKT activators as potential treatment for MLC patients.

Methods

Sex as a biological variable

In the zebrafish experiments sex was not considered as a biological variable since only larval stages were used (not yet undergone sexual determination). In the mouse experiments we examined male and female animals, and similar findings are reported for both sexes. For embryonic tissue samples no determination of sexes was possible. For the human participants, MLC affects patients from different genetic ancestries, and male and female are equally. Here we present 7 male and 3 female patients of European and Asian background.

KIF11 variants and in silico analysis

All the relative genomic and protein positions of *KIF11*/EG5 reported here correspond to the KIF11 NM_004523.4 transcript (ENST00000260731.5) and P52732 Uniprot protein accession ID. The genomic coordinated reported refer to the GRCh38/hg38 human genome reference (Supplemental Table 3). The pathogenicity was predicted by the Combined Annotation Dependent Depletion tool (56) and allele frequency checked in gnomAD databases (57). Variants were validated in accordance with ACMG and ACGS best practice guidelines: (ACGS 2024 variant interpretation guidelines: https://www.acgs.uk.com/media/12533/uk-practice-guidelines-for-variant-classification-v12-2024.pdf).

DNA and RNA/cDNA Analysis of the Splice Variant

To analyse the c.2922G>A variant reported in three of the index cases peripheral blood was obtained from individual F5-II.1. DNA was extracted using a standard chloroform ethanol procedure. Sequencing of DNA was performed using *KIF11* (NM_004523.4) forward primer 5'-caggtagcaagactgatcctca-3' and reverse primer 5'-cggggtaagattgaggggta-3' covering exon 20. RNA was collected using PAXgene Blood RNA tubes (PreAnalytiX, Hombrechtikon, Switzerland) and total RNA extracted using the PAXgene blood RNA Kit (PreAnalytix). DNAse treatment was performed to eliminate genomic DNA and cDNA synthesized from the RNA with a SuperScript II Reverse Transcriptase using about 400 ng RNA and 50 ng random primers (Invitrogen, Carlsbad, CA, USA). Sequencing of cDNA was performed using primers which span exons 19 to 22 of *KIF11* (NM_004523.4): Forward 5'-GGCAGCTCATGAGAAACAGC-3' and Reverse 5'-GCGAGCCCAGATCAACCTTT-3'. All PCR products were sequenced using BigDye Terminator v3.1 chemistry (Life Technologies, Carlsbad, CA, USA) and an ABI3130xla Genetic Analyzer (Life Technologies). Sequencing traces were visually inspected in FinchTV v1.4 (Geospiza). The protein prediction tool Expasy (www.expasy.org) was used to confirm the effect of the splice-site variant on the protein sequence.

Generation of lymphoblastoid cell lines from MLC patients and analysis of KIF11 (EG5) expression levels in blood and lymphoblastoid cell lines

Four patients from families F1 and F2 with MLC presenting with congenital, bilateral pedal lymphedema and two controls were selected for the generation of lymphoblastoid cells to analyse *KIF11* expression. Epstein-Barr virus (EBv) transformation was used for the generation of lymphoblastoid cell lines from the patients' peripheral blood lymphocytes at the Culture Collections, Public Health England, Porton Down. For the analysis of *KIF11* expression levels, qPCR was performed in total RNA samples extracted from blood and saliva. Extraction of RNA from blood samples was performed following the instructions of the Paxgene Blood RNA kit (PreAnalytiX 762154). Samples were eluted in 80µl of elution buffer provided by the kit and stored at -80°C until analysis. Extraction of RNA from saliva samples was done following the Oragene (OGR-500) collection protocol followed up from the Qiagen microkit RNA kit. RNA quality and concentration were assessed using Nanodrop. All RNA obtained was reverse transcribed using oligo dT (SuperScript III First-Strand Synthesis System 18080-051, Invitrogen). Gene expression levels were analysed using Platinum SYBR Green qPCR super mix-UDG with ROX reagent (QIAGEN) and a 7900 HT Fast Real-Time PCR System thermocycler (Applied Biosystems) following the manufacturer's instructions. Relative gene expression levels were normalized to GAPDH. Specific primers designed for each of the variants (underlined bases showing nucleotide changes) plus primers for wildtype and mutant alleles are: L347Efs*8: CTCTCAATCTTGAGGAAACTC / CTCTCAATCTTGAGGAAACTG / CTGATTCACTTCAGGCTTATTC; R387*: CGGGCTGCAGCAAGATCTCG / CGGGCTGCAGCAAGATCTCA / CTGAAGTGAATCAGAAACTC.

Validation of the qPCR was performed using cDNA in which the R387* variant was introduced by site-directed mutagenesis with the QuickChange XL site-directed mutagenesis kit (Stratagene 200517). Sequences were verified by Sanger sequencing analysis. Lymphoblastoid cells lines were cultured in suspension in RPMI 1640 supplemented with 2mM Glutamine and 20% Foetal Bovine Serum (FBS). Two independent EBv B cell lines were used as control (a gift from Dr. Nancy Hogg, Cancer Research UK London Research Institute, now part of the Francis Crick Institute, London, UK). Eg5 monoclonal antibodies against the N-terminal (CC10014, Cell Applications or NB500-181, Novus Biologicals) were used in the western blots and β-Actin was used as an internal control.

Isolation of intestinal biopsy from an MLC patient and analysis of lymphatic endothelial markers

An MLC patient presenting with failure to thrive, dysphagia and intermittent diarrhea and vomiting was subjected to endoscopy and intestinal biopsies taken for analysis by the Pathology Department at his local hospital. The intestinal biopsy, H&E and immunohistochemistry images were a gift from Dr Femke Piersma (Rems-Murr Kliniken,

Winnenden, Germany) and Dr Tränkenschuh (Robert Bosch Klinikum, Stuttgart, Germany). Subsequent immunofluorescence staining for epithelial and endothelial markers on 5µm tissue sections was performed according to the standard immunofluorescence histology protocol. Briefly, fixed tissue sections were washed and blocked (10% chicken serum, 0.3% Triton X-100 in PBS). Following blocking, tissue sections were incubated for 1 hour with primary antibodies (diluted in 1% BSA, 1% chicken serum, 0.3% Triton X-100 in PBS), washed thrice in PBS-T (0.1% Tween20 in PBS) and finally incubated in Alexa dye–conjugated secondary antibodies (Life Technologies). After sample mounting in Mowiol (Calbiochem, 475904), samples were imaged using a Zeiss LSM 980 confocal microscope (25x oil, NA = 0.8).

RNAscope in situ hybridization in human fetal tissue

The human tissue was collected at developmental stages ranging from CS12 to CS22. Tissues were primarily fixed in 10% PFA overnight at room temperature, and then secondarily fixed in Methacarn before they were processed using automated Excelsior AS (Thermo Scientific, A823-1005) to generate FFPE blocks. Sections were cut from the blocks at 8 µm using a manual rotary microtome (Leica microsystems RM2235, UK). Simultaneous RNA *in situ* hybridization was carried out using RNAscope Multiplex Fluorescent Reagent Kit v2 (Cat. No. 323100 and 323270, ACD) following the manufacture's protocol for FFPE tissue mounted on slides, with pre-treatment steps of Hydrogen Peroxide and Protease reagents (Cat. No. 322381, ACD) and target retrieval reagents for 20mins at 95ºC (Cat. No. 322000, ACD). The following RNAscope probes were designed and purchased from ACD: Hs-PDPN (Cat No. 539751), Hs-PROX1 (Cat No. 530241), VEGFR3 (Hs-FLT4) (Cat No. 552441-C2), and Hs-KIF11 (Cat No. 562641-C3). The probes were fluorescently labelled using OPAL 520 (Cat. No. FP1487001KT, PerkinElmer), OPAL 570 (Cat. No. FP1488001KT, PerkinElmer) and OPAL 650 dyes (Cat. No. FP1496001KT, PerkinElmer) for direct visualization under automated laser-scanning microscopy (Zeiss CellDiscoverer7, Carl Zeiss, Germany).

Mouse embryo collection, *mouse tissue collection, histology, immunofluorescence and RNAscope in situ hybridization*

See Supplementary Materials and Methods for details.

Zebrafish husbandry, genome editing, Ispinesib treatment, imaging and quantification

See Supplementary Materials and Methods for details.

Lymphatic endothelial cell culture, siRNA transfection and Ispinesib treatment

Human dermal LECs (HDLECs) (C-12217 or C-12216, PromoCell) were cultured and maintained in endothelial cell growth medium MV2 (C-22022, PromoCell) with FCS-based

supplement mix (C-39226) and recombinant human VEGFC 50ng/ml (2179-VC-025, R&D Systems). HDLECs single donor lots used in this study as follows: Lot 481Z001.2 (female), Lot 477Z011 and Lot 470Z021.2. Transfection of cells with siRNA *KIF11* #6 (NM_004523, SI02653693, target sequence 5'-ACGGAGGAGATAGAACGTTTA-3'), siRNA *KIF11* #7 (NM_004523, SI026533770, target sequence 5'-GCCGATAAGATAGAAGATCAA-3'), siRNA *PROX1* #8 (NM_002763, SI04372998, target sequence 5'-GACCTACTTCTCCGACGTAAA-3'), siRNA *FOXC2* #7 (NM_005251, SI03074834, target sequence 5'-CCAGAACGCGCCCGAGAAGAA-3') or siRNA 'All starts' negative control (1027281, Qiagen) was performed with Lipofectamine 2000 (Life Technologies) following the manufacturer's recommendations. Ispinesib (Tocris), a specific EG5 antagonist, was used at various concentrations and exposure times depending on the nature of the experiment. DMSO was used as vehicle.

Lymphatic endothelial cell functional assays

LECs were used in various functional assays such as transwell migration, wound healing, single cell migration tracking and spheroid sprouting assays. See Supplementary Materials and Methods for details.

Statistical analysis

Prism 9.0 software (GraphPad) was used for all statistical assessments apart from the single cell migration tracking done with R. Statistical significance between two groups was assessed by unpaired parametric two-tailed t-test. Statistically analysed data are presented as mean ± SEM or mean ± SD as specified for each analysis (described in the figure legends). Differences were considered significant when $p < 0.05$.

Study approval

Six index cases and affected family members with variants in *KIF11* were included in the study. Two were previously described (3) and four were direct referrals from clinicians. For the latter cases *KIF11* variants were detected by exome sequencing in the respective molecular genetics services and inheritance check if parental DNA was available. Ethical approval was given by the South West London Research Ethics Committee (REC Ref: 05/Q0803/257 and 14/LO/0753) or by Charité Ethics committee (EA4/214/19 'Molekulare und Moprhpogenetische Mechanismen der Lymphödementwicklung') and written informed consent was obtained from all participants.

Human embryonic tissue was obtained from the MRC/Wellcome-Trust funded Human Developmental Biology Resource (HBDR, http://www.hdbr.org), with appropriate maternal written consent and approval from the Newcastle and North Tyneside NHS Health Authority

Joint Ethics Committee. HDBR is regulated by the UK Human Tissue Authority (HTA; www.hta.gov.uk) and operates in accordance with the relevant HTA Codes of Practice.

Zebrafish work was conducted in compliance with animal ethics committees at the Peter MacCallum Cancer Centre and The University of Melbourne. All mouse procedures were approved by the German Federal Authorities (LaGeSo, Berlin; license number ZH120) and conducted in accordance with institutional, state, and government regulations.

Data availability

Source Data is provided in the Supporting Data Values XLS file accompanying this manuscript; available online. Data used to generate Figure 3B, Supplemental Figure 2 and Supplemental Figure 3, D-G were derived from sources in the public domain.

Author contributions

Conceptualization: S.J., P.M., S.M., S.M-A., P.O.; Project administration: S.M-A., P.O.; Investigation: K.O., R.Y.B., I.M-C., R.C.S.B., M.M., S.U., N.R.H., E.S., A.A., C.K., K.G., T.M., S.M-A.;, Formal analysis: KO, S.E.D., E.S., D.G., J.D.R.C, K.S.O., B.M.H., T.M., R.H., S.M-A., P.O.; Resources: M.O., D.W., A.E., K.K., K.G., B.M.H., R.H., S.M., P.O.; Writing – original draft: K.O., S.M-A., P.O.; Writing – review & editing: All authors. Supervision: S.J., P.M., K.S.O., B.M.H., T.M., R.H., S.M., S.M-A., P.O.; Funding acquisition: S.J., P.M., S.M., P.O.

Acknowledgements

We extend our thanks to the patients and their families, and to the 'KIF11Kids Association' in Germany. This work was supported by the British Heart Foundation (BHF) [SP/13/5/30288 and FS/15/39/31526] and a joint grant from the Medical Research Council (MRC) and the British Heart Foundation (BHF) [MR/P011543/1 and RG/17/7/33217]. SMA was supported by a research fellowship from the Rosetrees Trust [StGeorges-21\2] and St George's Hospital Charity [RES 20-21 003]. We thank Dr Femke Piersma (Rems-Murr Kliniken, Winnenden) and Dr Tränkenschuh (Robert Bosch Klinikum, Stuttgart) for providing the patient intestinal biopsy, H&E and immunohistochemistry images and interpretation, and Dr Sue Heenan (St George's University Hospital, London) for the lymphoscintigraphy images. The human embryonic and fetal material was provided by the Joint MRC / Wellcome (MR/R006237/1) Human Developmental Biology Resource (www.hdbr.org). We thank Dr Anna Oszmiana (University of South Australia) for sharing the ChIP-seq data and Mr Scott Paterson (University of Melbourne) for generating figures for the zebrafish work.

References

1. Jones GE, Ostergaard P, Moore AT, Connell FC, Williams D, Quarrell O, et al. Microcephaly with or without chorioretinopathy, lymphoedema, or mental retardation (MCLMR): review of phenotype associated with KIF11 mutations. Eur J Hum Genet. 2014 -07;22(7):881–7.

2. Balikova I, Robson AG, Holder GE, Ostergaard P, Mansour S, Moore AT. Ocular manifestations of microcephaly with or without chorioretinopathy, lymphedema or intellectual disability (MCLID) syndrome associated with mutations in KIF11. Acta Ophthalmol. 2016 -02;94(1):92–8.

3. Ostergaard P, Simpson MA, Mendola A, Vasudevan P, Connell FC, van Impel A, et al. Mutations in KIF11 cause autosomal-dominant microcephaly variably associated with congenital lymphedema and chorioretinopathy. Am J Hum Genet. 2012 -02-10;90(2):356–62.

4. Wang Y, Smallwood PM, Williams J, Nathans J. A mouse model for kinesin family member 11 (Kif11)-associated familial exudative vitreoretinopathy. Hum Mol Genet. 2020 -05-08;29(7):1121–31.

5. Gonzalez T, Tyler RC, Schilter KF, McCarrier J, Muriello M, Basel D, et al. KIF11 Variants Associated With Novel Renal System Involvement-Two Cases That Expand the Phenotypic Spectrum of Microcephaly With or Without Chorioretinopathy, Lymphedema, or Impaired Intellectual Development. Am J Med Genet A. 2024 -10-15:e63903.

6. Sawin KE, LeGuellec K, Philippe M, Mitchison TJ. Mitotic spindle organization by a plus-end-directed microtubule motor. Nature. 1992 -10-08;359(6395):540–3.

7. Konjikusic MJ, Gray RS, Wallingford JB. The developmental biology of kinesins. Dev Biol. 2021 -01-01;469:26–36.

8. Chauvière M, Kress C, Kress M. Disruption of the mitotic kinesin Eg5 gene (Knsl1) results in early embryonic lethality. Biochem Biophys Res Commun. 2008 -08-08;372(4):513–9.

9. Castillo A, Justice MJ. The kinesin related motor protein, Eg5, is essential for maintenance of pre-implantation embryogenesis. Biochem Biophys Res Commun. 2007 -06-08;357(3):694–9.

10. Wakana Y, Villeneuve J, van Galen J, Cruz-Garcia D, Tagaya M, Malhotra V. Kinesin-5/Eg5 is important for transport of CARTS from the trans-Golgi network to the cell surface. J Cell Biol. 2013 -07-22;202(2):241–50.

11. Venere M, Horbinski C, Crish JF, Jin X, Vasanji A, Major J, et al. The mitotic kinesin KIF11 is a driver of invasion, proliferation, and self-renewal in glioblastoma. Sci Transl Med. 2015 -09-09;7(304):304ra143.

12. Swarnkar S, Avchalumov Y, Raveendra BL, Grinman E, Puthanveettil SV. Kinesin Family of Proteins Kif11 and Kif21B Act as Inhibitory Constraints of Excitatory Synaptic Transmission Through Distinct Mechanisms. Sci Rep. 2018 -11-27;8(1):17419.

13. Zalenski AA, Majumder S, De K, Venere M. An interphase pool of KIF11 localizes at the basal bodies of primary cilia and a reduction in KIF11 expression alters cilia dynamics. Sci Rep. 2020 -08-18;10(1):13946.

14. Ran J, Li H, Zhang Y, Yu F, Yang Y, Nie C, et al. A non-mitotic role for Eg5 in regulating cilium formation and sonic hedgehog signaling. Sci Bull (Beijing). 2021 -08-30;66(16):1620–3.

15. Wei N, Yu Y, Yang Y, Wang X, Zhong Z, Chen X, et al. Inhibitions and Down-Regulation of Motor Protein Eg5 Expression in Primary Sensory Neurons Reveal a Novel Therapeutic Target for Pathological Pain. Neurotherapeutics. 2022 July 1;19(4):1401–13.

16. Schlögel MJ, Mendola A, Fastré E, Vasudevan P, Devriendt K, de Ravel TJL, et al. No evidence of locus heterogeneity in familial microcephaly with or without chorioretinopathy, lymphedema, or mental retardation syndrome. Orphanet J Rare Dis. 2015 -05-02;10:52.

17. Gordon K, Varney R, Keeley V, Riches K, Jeffery S, Van Zanten M, et al. Update and audit of the St George's classification algorithm of primary lymphatic anomalies: a clinical and molecular approach to diagnosis. J Med Genet. 2020 -10;57(10):653–9.

18. Joyce S, Gordon K, Brice G, Ostergaard P, Nagaraja R, Short J, et al. The lymphatic phenotype in Noonan and Cardiofaciocutaneous syndrome. Eur J Hum Genet. 2016 -05;24(5):690–6.

19. Scholey JE, Nithianantham S, Scholey JM, Al-Bassam J. Structural basis for the assembly of the mitotic motor Kinesin-5 into bipolar tetramers. Elife. 2014 -04-08;3:e02217.

20. Truebestein L, Leonard TA. Coiled-coils: The long and short of it. Bioessays. 2016 -09;38(9):903–16.

21. Exertier P, Javerzat S, Wang B, Franco M, Herbert J, Platonova N, et al. Impaired angiogenesis and tumor development by inhibition of the mitotic kinesin Eg5. Oncotarget. 2013 -12;4(12):2302–16.

22. Hägerling R, Pollmann C, Andreas M, Schmidt C, Nurmi H, Adams RH, et al. A novel multistep mechanism for initial lymphangiogenesis in mouse embryos based on ultramicroscopy. EMBO J. 2013 -03-06;32(5):629–44.

23. Kazenwadel J, Venugopal P, Oszmiana A, Toubia J, Arriola-Martinez L, Panara V, et al. A Prox1 enhancer represses haematopoiesis in the lymphatic vasculature. Nature. 2023 -02;614(7947):343–8.

24. Moore JE, Purcaro MJ, Pratt HE, Epstein CB, Shoresh N, Adrian J, et al. Expanded encyclopaedias of DNA elements in the human and mouse genomes. Nature. 2020 -07;583(7818):699–710.

25. González-Loyola A, Bovay E, Kim J, Lozano TW, Sabine A, Renevey F, et al. FOXC2 controls adult lymphatic endothelial specialization, function, and gut lymphatic barrier preventing multiorgan failure. Science Advances. 2021 July 16;7(29):eabf4335.

26. Petkova M, Kraft M, Stritt S, Martinez-Corral I, Ortsäter H, Vanlandewijck M, et al. Immune-interacting lymphatic endothelial subtype at capillary terminals drives lymphatic malformation. Journal of Experimental Medicine. 2023 January 23;220(4):e20220741.

27. Grimm L, Mason E, Yu H, Dudczig S, Panara V, Chen T, et al. Single-cell analysis of lymphatic endothelial cell fate specification and differentiation during zebrafish development. EMBO J. 2023 -03-13:e112590.

28. Ferenz NP, Gable A, Wadsworth P. Mitotic functions of kinesin-5. Semin Cell Dev Biol. 2010 -05;21(3):255–9.

29. Garcia-Saez I, Skoufias DA. Eg5 targeting agents: From new anti-mitotic based inhibitor discovery to cancer therapy and resistance. Biochem Pharmacol. 2021 -02;184:114364.

30. Jafree DJ, Long DA, Scambler PJ, Ruhrberg C. Mechanisms and cell lineages in lymphatic vascular development. Angiogenesis. 2021 -05;24(2):271–88.

31. Phan TP, Maryniak AL, Boatwright CA, Lee J, Atkins A, Tijhuis A, et al. Centrosome defects cause microcephaly by activating the 53BP1-USP28-TP53 mitotic surveillance pathway. EMBO J. 2021 -01-04;40(1):e106118.

32. Wigle JT, Harvey N, Detmar M, Lagutina I, Grosveld G, Gunn MD, et al. An essential role for Prox1 in the induction of the lymphatic endothelial cell phenotype. EMBO J. 2002 -04-02;21(7):1505–13.

33. Petrova TV, Mäkinen T, Mäkelä TP, Saarela J, Virtanen I, Ferrell RE, et al. Lymphatic endothelial reprogramming of vascular endothelial cells by the Prox-1 homeobox transcription factor. EMBO J. 2002 -09-02;21(17):4593–9.

34. Hong Y, Harvey N, Noh Y, Schacht V, Hirakawa S, Detmar M, et al. Prox1 is a master control gene in the program specifying lymphatic endothelial cell fate. Dev Dyn. 2002 -11;225(3):351–7.

35. Cha B, Geng X, Mahamud MR, Fu J, Mukherjee A, Kim Y, et al. Mechanotransduction activates canonical Wnt/β-catenin signaling to promote lymphatic vascular patterning and the development of lymphatic and lymphovenous valves. Genes Dev. 2016 -06-15;30(12):1454–69.

36. Baluk P, Fuxe J, Hashizume H, Romano T, Lashnits E, Butz S, et al. Functionally specialized junctions between endothelial cells of lymphatic vessels. J Exp Med. 2007 -10-01;204(10):2349–62.

37. Frye M, Stritt S, Ortsäter H, Hernandez Vasquez M, Kaakinen M, Vicente A, et al. EphrinB2-EphB4 signalling provides Rho-mediated homeostatic control of lymphatic endothelial cell junction integrity. eLife. 2020 Sep 8;9.

38. Hägerling R, Hoppe E, Dierkes C, Stehling M, Makinen T, Butz S, et al. Distinct roles of VE-cadherin for development and maintenance of specific lymph vessel beds. EMBO J. 2018 -11-15;37(22):e98271.

39. Norden PR, Sabine A, Wang Y, Demir CS, Liu T, Petrova TV, et al. Shear stimulation of FOXC1 and FOXC2 differentially regulates cytoskeletal activity during lymphatic valve maturation. Elife. 2020 -06-08;9:e53814.

40. Ricci A, Carradori S, Cataldi A, Zara S. Eg5 and Diseases: From the Well-Known Role in Cancer to the Less-Known Activity in Noncancerous Pathological Conditions. Biochem Res Int. 2024;2024:3649912.

41. Sarica M, Gordon K, van Zanten M, Heenan SD, Mortimer PS, Irwin AG, et al. Lymphoscintigraphic Abnormalities Associated with Milroy Disease and Lymphedema-Distichiasis Syndrome. Lymphat Res Biol. 2019 -12;17(6):610–9.

42. Mellor RH, Hubert CE, Stanton AWB, Tate N, Akhras V, Smith A, et al. Lymphatic dysfunction, not aplasia, underlies Milroy disease. Microcirculation. 2010 -05;17(4):281–96.

43. Bernier-Latmani J, Cisarovsky C, Demir CS, Bruand M, Jaquet M, Davanture S, et al. DLL4 promotes continuous adult intestinal lacteal regeneration and dietary fat transport. J Clin Invest. 2015 -11-03;125(12):4572–86.

44. Betterman KL, Sutton DL, Secker GA, Kazenwadel J, Oszmiana A, Lim L, et al. Atypical cadherin FAT4 orchestrates lymphatic endothelial cell polarity in response to flow. J Clin Invest. 2020 -06-01;130(6):3315–28.

45. Cifarelli V, Eichmann A. The Intestinal Lymphatic System: Functions and Metabolic Implications. Cell Mol Gastroenterol Hepatol. 2019;7(3):503–13.

46. Guo Z, Huo X, Wu D, Hao B, Liao S. A Novel Variant of the KIF11 Gene, c.2922G>T, Is Associated with Microcephaly by Affecting RNA Splicing. Dev Neurosci. 2022;44(2):113–20.

47. Falnikar A, Tole S, Baas PW. Kinesin-5, a mitotic microtubule-associated motor protein, modulates neuronal migration. Mol Biol Cell. 2011 -05;22(9):1561–74.

48. Wang F, Lin SL. Knockdown of kinesin KIF11 abrogates directed migration in response to epidermal growth factor-mediated chemotaxis. Biochem Biophys Res Commun. 2014 -09-26;452(3):642–8.

49. Ganguly A, Yang H, Sharma R, Patel KD, Cabral F. The role of microtubules and their dynamics in cell migration. J Biol Chem. 2012 -12-21;287(52):43359–69.

50. Ganguly S, Williams LS, Palacios IM, Goldstein RE. Cytoplasmic streaming in Drosophila oocytes varies with kinesin activity and correlates with the microtubule cytoskeleton architecture. Proc Natl Acad Sci U S A. 2012 -09-18;109(38):15109–14.

51. Martinez-Corral I, Zhang Y, Petkova M, Ortsäter H, Sjöberg S, Castillo SD, et al. Blockade of VEGF-C signaling inhibits lymphatic malformations driven by oncogenic PIK3CA mutation. Nat Commun. 2020 -06-08;11(1):2869.

52. Chen Y, Tao S, Xu Z, Yin W, Zhang Y, Yin J, et al. Novel Akt activator SC-79 is a potential treatment for alcohol-induced osteonecrosis of the femoral head. Oncotarget. 2017 -05-09;8(19):31065–78.

53. Li D, March ME, Gutierrez-Uzquiza A, Kao C, Seiler C, Pinto E, et al. ARAF recurrent mutation causes central conducting lymphatic anomaly treatable with a MEK inhibitor. Nat Med. 2019 -07;25(7):1116–22.

54. Sheppard SE, March ME, Seiler C, Matsuoka LS, Kim SE, Kao C, et al. Lymphatic disorders caused by mosaic, activating KRAS variants respond to MEK inhibition. JCI Insight. 2023 -05-08;8(9):e155888.

55. Waters SB, Dominguez JR, Cho H, Sarich NA, Malik AB, Yamada KH. KIF13B-mediated VEGFR2 trafficking is essential for vascular leakage and metastasis in vivo. Life Sci Alliance. 2022 -01;5(1):e202101170.

56. Rentzsch P, Witten D, Cooper GM, Shendure J, Kircher M. CADD: predicting the deleteriousness of variants throughout the human genome. Nucleic Acids Research. 2019 -01-08;47(D1):D886–94.

57. Karczewski KJ, Francioli LC, Tiao G, Cummings BB, Alföldi J, Wang Q, et al. The mutational constraint spectrum quantified from variation in 141,456 humans. Nature. 2020 May 1;581(7809):434–43.

58. Martin-Almedina S, Martinez-Corral I, Holdhus R, Vicente A, Fotiou E, Lin S, et al. EPHB4 kinase-inactivating mutations cause autosomal dominant lymphatic-related hydrops fetalis. J Clin Invest. 2016 -08-01;126(8):3080–8.

Family - Individual	F1-II.1		F3-II.2		F3-II.1		Control
Lower limb	Right	Left	Right	Left	Right	Left	Normal values
Tracer retention in foot at 2hrs (%)	>99	>99	89.8	96.4	97.7	70.1	<80
Uptake in ilioinguinal nodes at 2hrs (%)	0.2	0.2	0.4	0.1	0.1	2.6	>12
KIF11 variant	c.1159C>T		c.2680C>T		c.2680C>T		
Predicted EG5 protein change	p.(Arg387*)		p.(Gln894*)		p.(Gln894*)		
Sex (age [years] at time of scan)	Female (10)		Male (35)		Male (31)		

Table 1: Quantification figures 2 hours post injection. Quantification figures are given as % of radionuclide tracer retention in right and left foot and tracer uptake in the ilioinguinal nodes. Values for an individual with a normal lymphatic system are also given in the table. Genetic variants and predicted protein changes are also shown, including the sex and age at the time of scan.

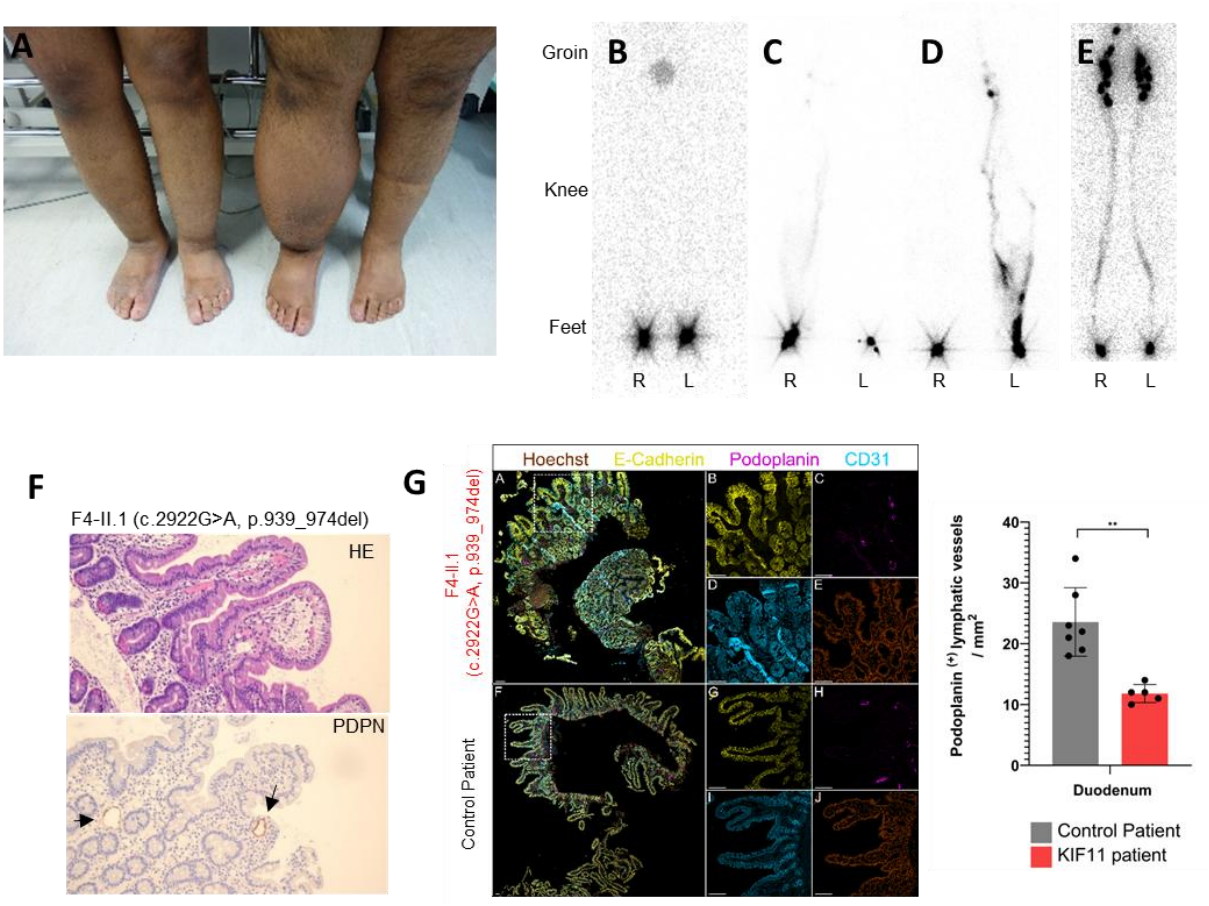

Figure 1: MLC patients show lymphatic abnormalities. (A) Photography of lower limbs of patients F3-II.1 and F3-II.2 showing asymmetrical lower limb lymphedema. **(B-E)** Lower limb lymphoscintigraphy 2 hours after injection of radionuclide (technetium-99) is used to image the lymphatic system (anterior view shown here). **(B)** Bilateral functional aplasia evidenced by no lymphatic drainage in either leg. **(C)** Significantly reduced function with rerouting in the right limb and functional aplasia of the left. **(D)** Functional aplasia of the right limb and abnormal tortuous tracts with patchy superficial re-routing on the left. **(E)** Unaffected subject with symmetrical transport of radionuclide tracer from injection sites in the feet up to the inguinal lymph nodes via main lymphatic vessels. **(F)** Intestinal biopsy of patient F4-II.1 with *KIF11* variant c.2922G>A; p.939_974del. H&E (HE) staining shows aberrant morphology of the lacteals, Podoplanin (PDPN) detected slightly enlarged lymphatic vessels (arrows). **(G)** Human duodenum sections derived from same patient as in (F) and an unaffected control were subjected to immunofluorescence staining. Selected magnifications (framed areas) depict staining for Hoechst (brown; E, J), E-cadherin (yellow; B, G), Podoplanin (magenta; C, H), CD31 (cyan; D, I). Scale bars represent 100 µm. Immunofluorescence staining revealed significantly reduced lymphatic vessel density compared to healthy control samples based on Podoplanin positive area per mm^2 tissue area. Two tailed Student t-test $p<0.01$. (E) is a

historical standard taken from authors' archive: "Methods of imaging the lymphatic system" by City St. George's University of London licensed under CC BY-SA-4.0, and also published in (58).

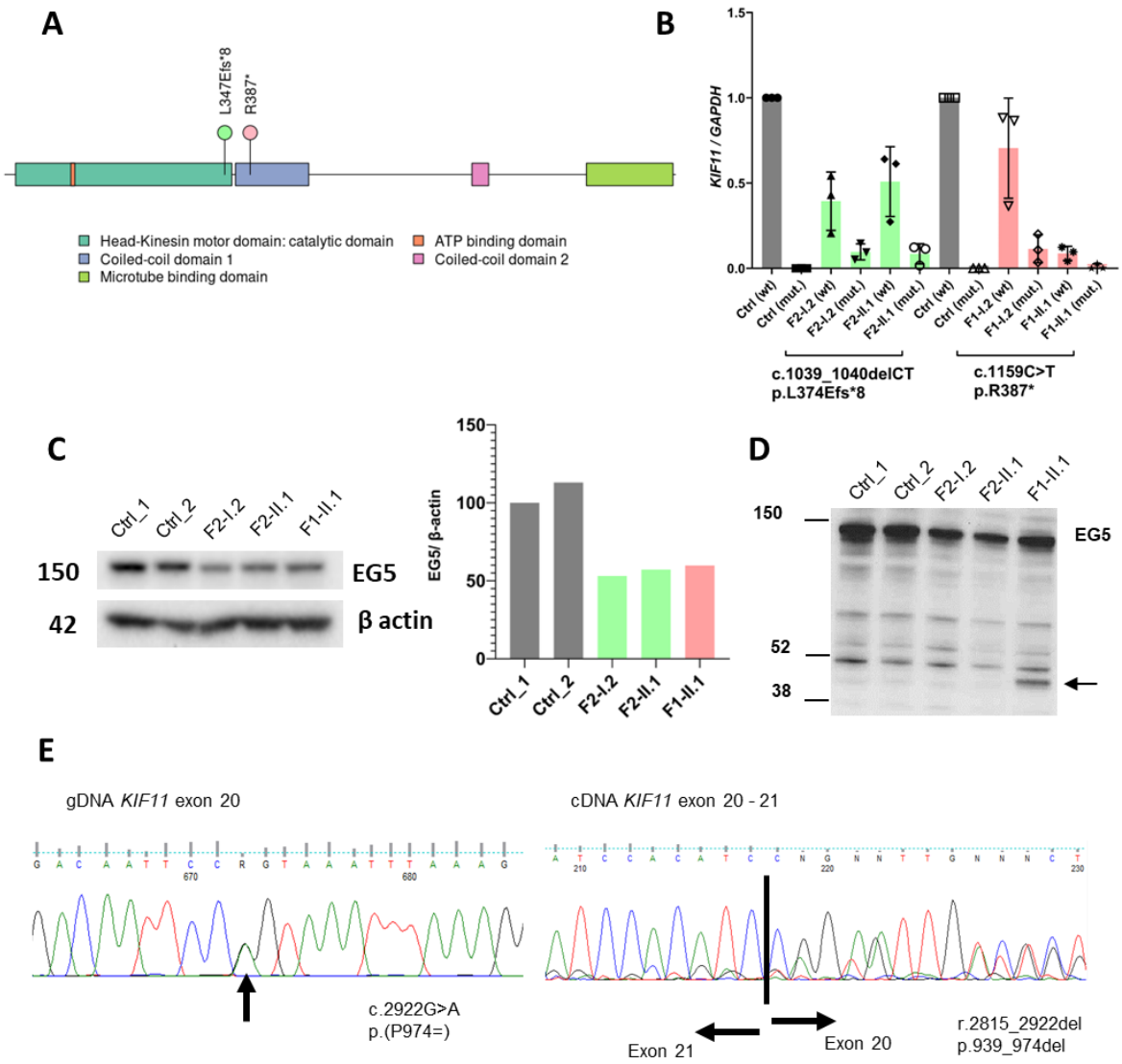

Figure 2: Reduced expression of *KIF11* (EG5) and splicing abnormalities suggest haploinsufficiency as the disease mechanism in MLC. (A) EG5 (*KIF11*) protein domain structure indicating the position of the MLC variants p.L347Efs*8 and p.R387*. **(B)** qRT-PCR analysis of blood using allele-specific primers (wt: wild type allele, mut: patient variant allele) showing strong reduction, but not a complete absence of the mutant mRNA in all samples (F2-I.2, F2-II.1, F1-I.2 and F1-II.1), suggesting nonsense mediated RNA decay. wt *KIF11* mRNA levels decreased by up to 50% in patients compared to controls. Data represent average relative expression (n=3 experiments) ± SD. **(C)** Western blot analysis of lymphoblastoid cell lines lysates indicate approximately 50% reduction in the levels of wt EG5 protein (119kDa) in the patient samples (F2-I.2, F2-II.1, and F1-II.1) using C-terminal binding EG5 antibody (NB500-181, Novus Biologicals). Average of 2 technical repeats of identical biological materials is shown with beta-actin as loading control. **(D)** Western blot analysis with an N-terminal binding anti-EG5 antibody (CC10014, Cell Applications, USA) showed the presence of a truncated protein of the expected size in patient F1-I.2 (arrow). The position of molecular

mass markers (in kDa) is indicated on the left of the gel. **(E)** Left panel: Sanger sequencing of gDNA from proband F5-II.1. PCR product shows a compound peak in exon 20, which is the synonymous *KIF11* c.2922G>A; p.(P974=) variant. Right panel: Sanger sequencing of cDNA from F5-II.1. Black line indicates the boundary between the last base of exon 20 and first base of exon 21. Notice the heteroduplex in exon 20 indicating exon skipping. Analysis of the full trace identified a loss of the last 108 bases in exon 20 (r.2815_2922del) which is predicted to lead to a shorter EG5 protein similar to that of the synonymous variant c.2922G>T as shown by others (46).

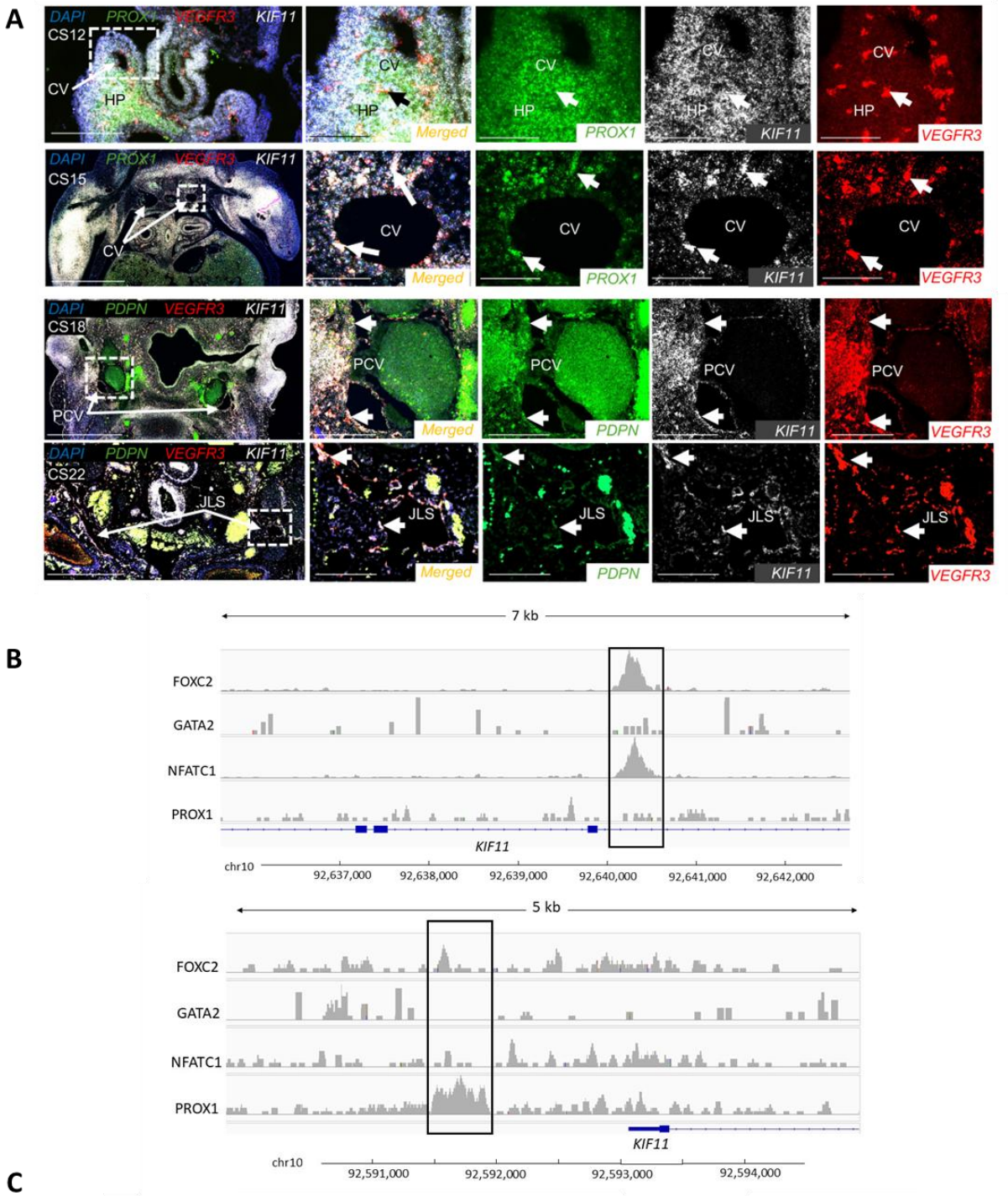
A
DAPI PROX1 VEGFR3 KIF11
CS12
CV
HP
Merged
PROX1
KIF11
VEGFR3
CS15
PDPN
CS18
PCV
CS22
JLS
B
7 kb
FOXC2
GATA2
NFATC1
PROX1
KIF11
chr10
92,637,000
92,638,000
92,639,000
92,640,000
92,641,000
92,642,000
5 kb
92,591,000
92,592,000
92,593,000
92,594,000
C
siRNA C
siRNA PROX1
siRNA FOXC2
PROX1/GAPDH
KIF11/GAPDH
FOXC2/GAPDH
24 Hours
48 Hours

Figure 3: *KIF11* expression during human embryonic development and transcriptional control in adult lymphatic endothelial cells. (A) Human embryonic slides corresponding with different embryonic developmental Carnegie stages (CS12, CS15, CS18 and CS22) were hybridised with fluorescence probes for *KIF11* (white), *PROX1* or *PDPN* (green) and *FLT4* (red). Magnified regions marked with a square box in overview images contain the pre-cardinal veins (PCV), cardinal veins (CV) and jugular lymphatic sacs (JLS), and arrows point to regions of co-expression between *KIF11* and lymphatic endothelial marker expression. HP, hepatic primordia. Scale bar 200 μm. **(B)** ChIP-seq analysis in cultured human dermal LECs identifies an intronic region of *KIF11* bound by FOXC2 and NFATC1 (top panel) and PROX1 binding 1.3kb upstream of *KIF11* promoter (bottom panel). **(C)** LECs were treated with siRNA *PROX1* or siRNA *FOXC2* and *KIF11* expression was evaluated by qPCR. Bars represent mean relative expression ± SEM from n=3 experiments. **P<0.01, ***P<0.001, ****P<0.0001. Two-tailed unpaired Student's t-test.

A

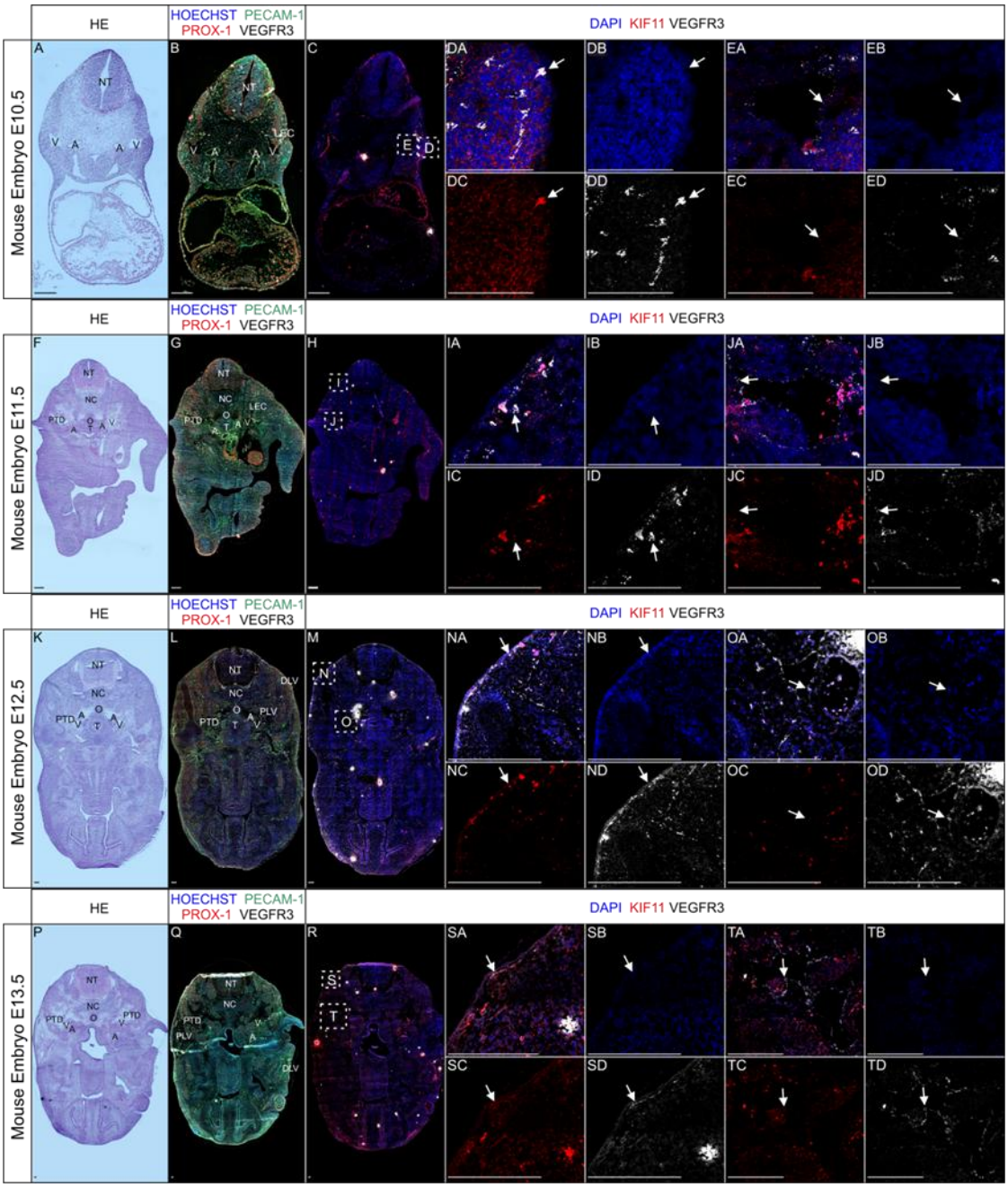
HE
HOECHST PECAM-1
PROX-1 VEGFR3
DAPI KIF11 VEGFR3
Mouse Embryo E10.5
Mouse Embryo E11.5
Mouse Embryo E12.5
Mouse Embryo E13.5
NT
NC
LEC
PTD
PLV
DLV

B

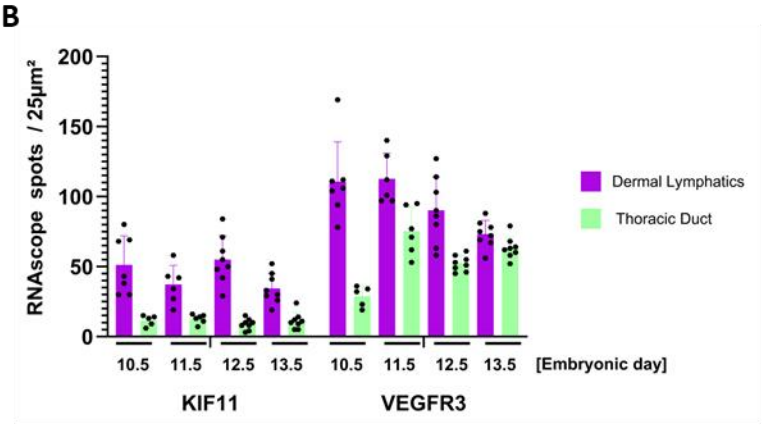
RNAscope spots / 25µm²
200
150
100
50
0
10.5
11.5
12.5
13.5
[Embryonic day]
KIF11
VEGFR3
Dermal Lymphatics
Thoracic Duct

C

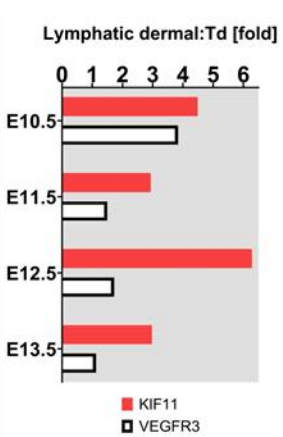
Lymphatic dermal:Td [fold]
0 1 2 3 4 5 6
E10.5
E11.5
E12.5
E13.5
KIF11
VEGFR3

Figure 4: *Kif11* co-expression with *Flt4*-positive lymphatic vessels during mouse embryonic development. (A) Mouse embryonic sections from developmental stages E10.5 to E13.5 were processed by H&E staining (panels A, F, K, P), immunofluorescence staining (panels B, G, L, Q), or RNA hybridization (panels C, H, M, R). Selected magnified (framed) areas highlight embryonic regions containing dermal lymphatics (panels D, I, N, S) and the thoracic duct (panels E, J, O, T). These regions were imaged using DAPI staining (blue; channel 2) as well as for *Kif11* (red; channel 3) and *Flt4* (white; channel 4) mRNA expression; merged images are shown in panels DA, EA, IA, JA, NA, OA, SA, TA. Arrowheads indicate areas with co-expression of *Kif11* and *Flt4* mRNA. Additional labeling was added to facilitate the understanding of the embryonic anatomy: A – Artery; DLV – Dermal Lymphatic Vessels; LEC – Initial Lymphatic Endothelial Cell; NC – Notochord; NT – Neural Tube; O – Oesophagus; T – Trachea; PLV – Peripheral Lymphatic Vessels; PTD – Primordial Thoracic Duct; V – Vein. Scale bars represent 100 µm. **(B)** Quantification of *Kif11* and *Flt4* mRNA signals from dermal (purple) and thoracic duct (light green) of different stages of mouse embryo development. RNAscope signals were measured from 6-8 different areas of 25um^2 **(C)** Bar chart represents *Kif11* (red) and *Flt4* (VEGFR3) (white) mRNA signal ratio in dermal versus thoracic duct (Td) during different stages of mouse embryo development.

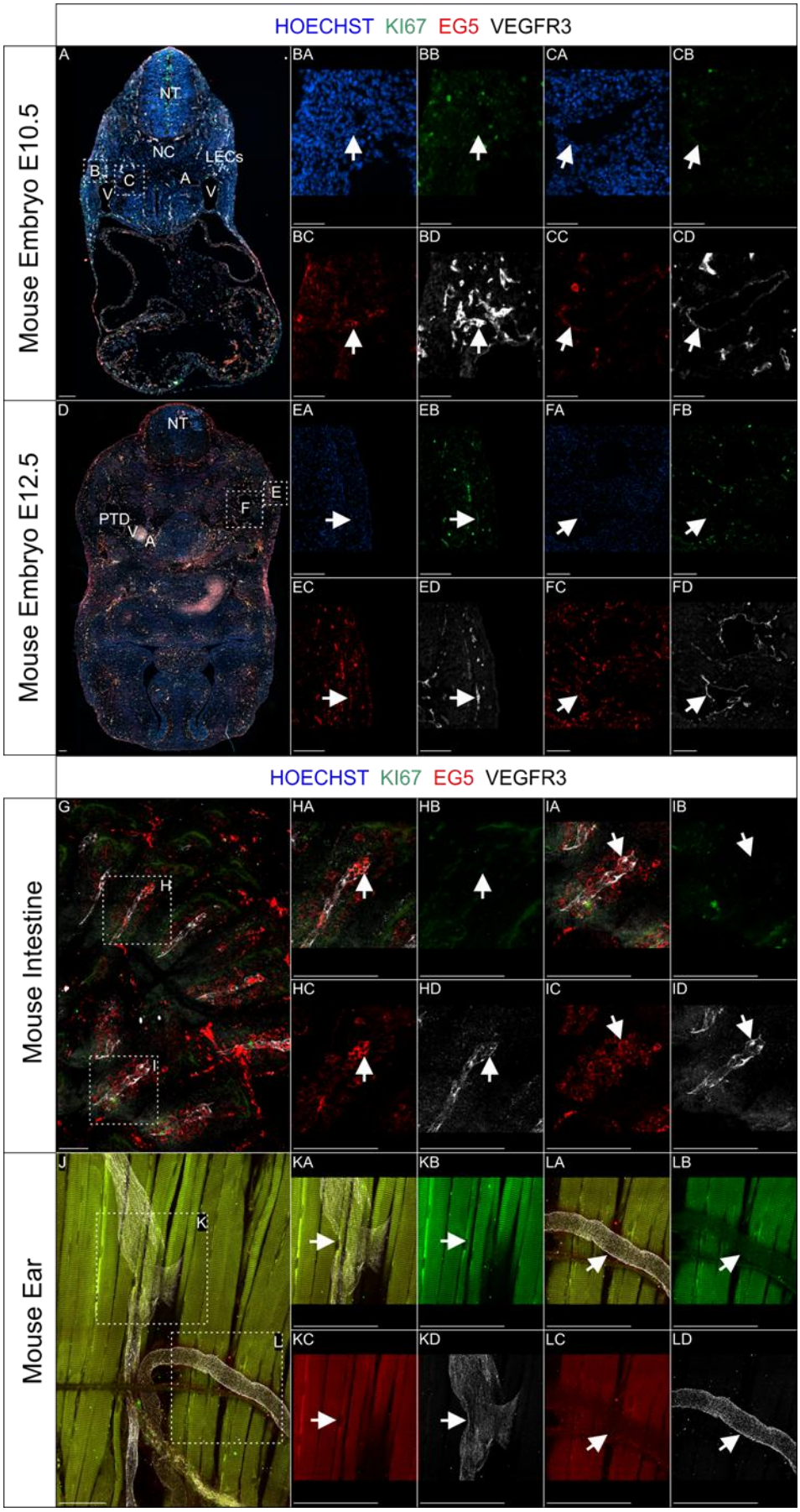
HOECHST KI67 EG5 VEGFR3
Mouse Embryo E10.5
Mouse Embryo E12.5
Mouse Intestine
Mouse Ear
NT
NC
LECs
PTD
V
A
B
C
D
E
F
G
H
I
J
K
L
BA
BB
BC
BD
CA
CB
CC
CD
EA
EB
EC
ED
FA
FB
FC
FD
HA
HB
HC
HD
IA
IB
IC
ID
KA
KB
KC
KD
LA
LB
LC
LD

Figure 5: EG5 protein co-expression with VEGFR3-positive lymphatic vessels during mouse embryonic development and its expression pattern in adult mice. Mouse embryonic sections from different developmental stages (E10.5 and E12.5) were subjected to immunofluorescence staining (panels A and D, respectively). Selected magnified (framed) areas highlight regions containing dermal lymphatics (panels B and E) and the thoracic duct (panels C and F), which were imaged for DAPI (blue; channel 1), Ki67 (green; channel 2), EG5 (red; channel 3), and VEGFR3 (white; channel 4) protein expression. Additionally, whole-mount immunofluorescence staining was performed on intestinal and ear samples (panels G and J, respectively). Selected magnifications highlight regions with lacteals (panels H and I) and initial lymphatic vessels (panels K and L), also imaged for Ki67 (green; channel 2), EG5 (red; channel 3), and VEGFR3 (white; channel 4); merged images are shown in panels HA, IA, KA, and LA Arrowheads indicate areas with co-expression of EG5 and VEGFR3. Scale bars represent 100 µm. Additional labeling was added to facilitate the understanding of the embryonic anatomy: A – Artery; LEC – Initial Lymphatic Endothelial Cell; NC – Notochord; NT – Neural Tube; PLV – Peripheral Lymphatic Vessels; PTD – Primordial Thoracic Duct; V – Vein.

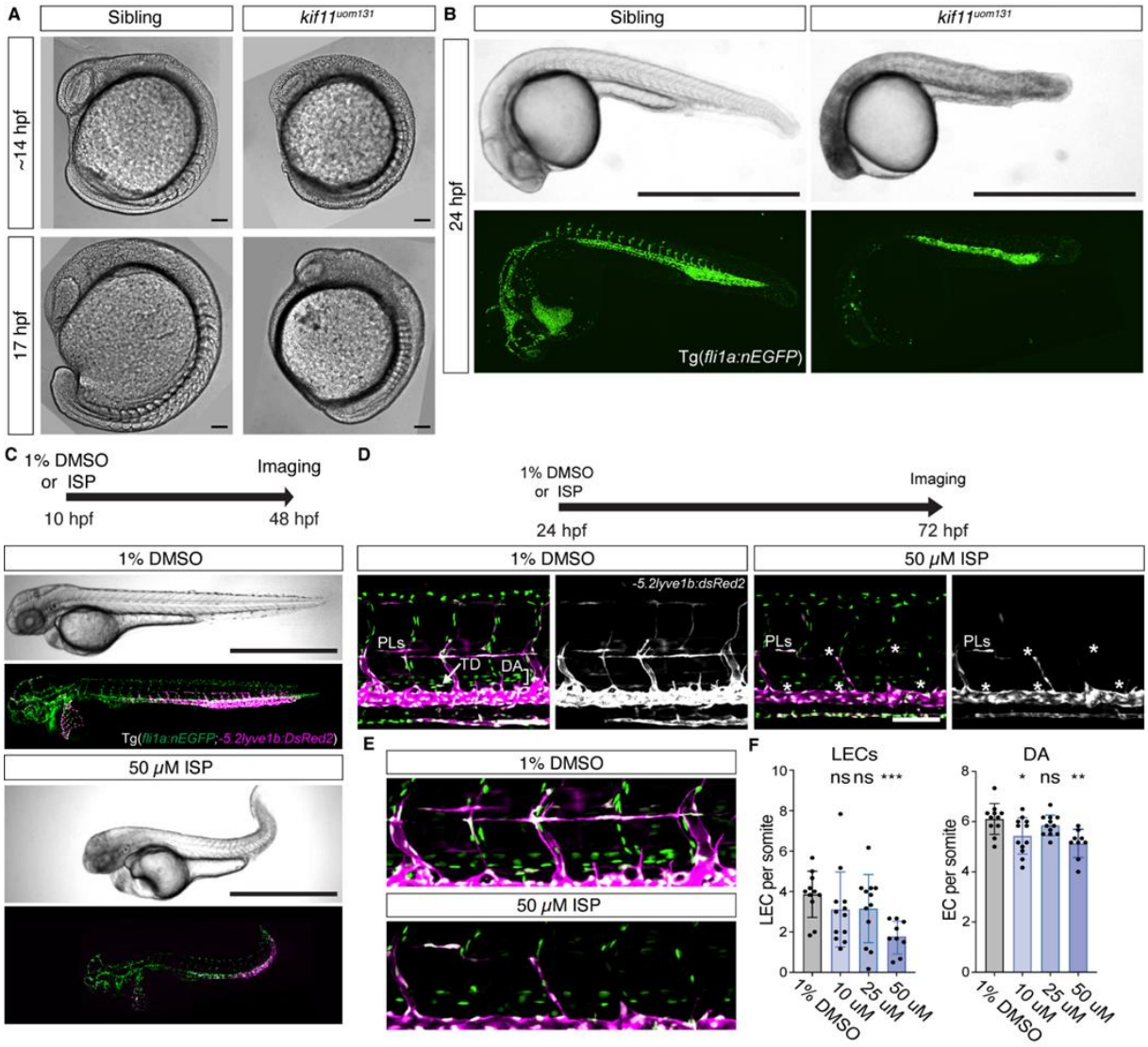

Figure 6: Genetic and pharmacological loss of *kif11* results in abnormal embryonic and vascular development in zebrafish. (A) Differential inference contrast (DIC) images of 14 and 17 hours post fertilization (hpf) sibling (*kif11*$^{+/+ \text{ or } +/uom131}$) and mutant embryos (*kif11*^{uom131}). Somite defects, brain necrosis and aberrant tail development are observable in 100% of mutants at both timepoints (n=8/8 mutants and n=0/19 sibling at 14 hpf and n=8/8 mutants and n=0/7 sibling at 14 and 17 hpf, respectively). Scale = 100μm. **(B)** Upper: Brightfield images of sibling and mutant embryos at 24 hpf. Brain necrosis and reduced embryo size are observable in mutants. Lower: Confocal maximum projection images of Tg(*fli1a:nEGFP*) embryos showing reduced intersegmental vessel sprouting and vascular development likely consistent with delayed embryonic development. (n=26/26 mutants and n=0/88 sibling). Scale =1mm**. (C)** Brightfield and confocal maximum projection images of DMSO control (upper) and treated (lower) embryos following exposure to 50μM Ispinesib (ISP) between 10–48 hpf. Tg(*fli1a:nEGFP;lyve1b:DsRed2)* used to visualise endothelial cells, veins and lymphatic progenitors. ISP treatment caused brain necrosis, pericardial oedema and aberrant tail

development (n=26/26 ISP-treated, n=27 1% DMSO). Scale =1mm. **(D)** Confocal maximum projection images of DMSO control or 50μM ISP-treated Tg(*fli1a:nEGFP;lyve1b:DsRed2)* embryos at 72 hpf. ISP treatment was from 24 to 72 hpf. 50μM ISP-treated embryos showed impaired lymphatic progenitor (PL) formation at the horizontal myoseptum (quantified in E). Scale =100μm. **(E)** Zoomed images of the DA and PLs from D. **(F)** Bar plots of EC numbers in the DA and PLs upon treatment with increasing ISP concentrations (EC numbers per somite are displayed). Reductions in both LECs and DA ECs were observed as shown. Statistics: Unpaired Student's t-test for normally distributed data and Mann-Whitney test for non-normally distributed data. (*, p=0.0261; **, p=0.0018; ***, p=0.0002; ns, non-significant) (n=11 1% DMSO, n=12 10μM ISP, n=12 25μM ISP, n=9 50μM ISP). TD, thoracic duct; DA, dorsal aorta; DA, dorsal aorta; EC, endothelial cell.

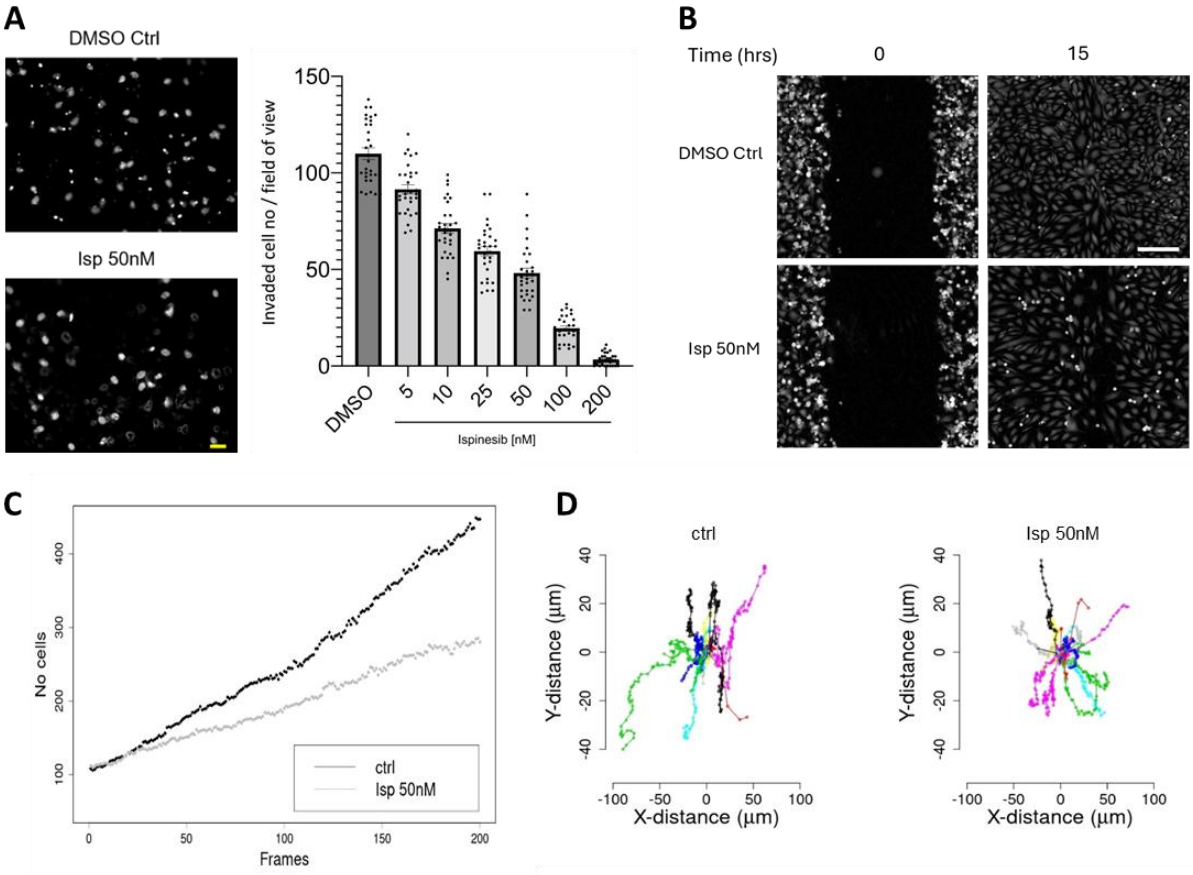
A
DMSO Ctrl
Isp 50nM
Invaded cell no / field of view
150
100
50
0
DMSO
5
10
25
50
100
200
Ispinesib [nM]
B
Time (hrs)
0
15
DMSO Ctrl
Isp 50nM
C
No cells
400
300
200
100
0
50
100
150
200
Frames
ctrl
Isp 50nM
D
ctrl
Isp 50nM
Y-distance (µm)
X-distance (µm)
40
20
0
-20
-40
-100
-50
0
50
100
E
VEGF-C stimulation (150ng/ml)
Ispinesib
DMSO
DMSO
25nM
50nM
100nM
Avg. sprout length (µm)
400
300
200
100
0
***
***
**
***
DMSO
+VEGF-C
25nM
50nM
100nM
Ispinesib [nM]
No. of sprouts / spheroid
24
20
16
12
8
4
0
***
ns
**
**
DMSO
+VEGF-C
25nM
50nM
100nM
Ispinesib [nM]

Figure 7: *KIF11* deficiency impairs LEC migration and sprouting. (A) 5 x 10^4 serum starved cells were plated per fibronectin-coated transwell chamber and given 10 hours to migrate in the presence of increasing concentrations of Ispinesib (Isp) (0 to 200 nM) before fixation and staining of the nuclei with DAPI. Resulting membranes (two examples given on the left) were scored for the movement of nuclei through the transwell membrane, and results represented in a plot (on the right). Error bars represent SD, n = 3 biological replicates (with 2 technical replicates per biological replicate). Scale bar 50 µm. **(B)** Single cell tracking migration assay follows wound closure ability over 15 hours in DMSO (Ctrl) and 50nM Ispinesib treated cells. Scale bar 200 µm. **(C)** Number of cells in experimental wound-window area for Ctrl and 50nM Ispinesib treated cells over time (frames). **(D)** Distance and direction of a subset of cells illustrated as star plots of cell tracks for Ctrl and 50nM Ispinesib treated cells. (B-D) One representative experiment is shown from n=2. **(E)** 3D spheroid sprouting assay. Sprouting was stimulated in LECs by VEGFC 150 ng/ml either in the presence of DMSO vehicle or several doses of Ispinesib (25, 50, 100nM). Average sprout length in µm (28 spheroids analysed) and total number of sprouts per spheroid (15 spheroids analysed) were quantified in each condition. One representative image is shown per condition from n=2 biological repeat. ns=not significant, *p<0.05, **p<0.01, ***p<0.001. Two-tailed unpaired Student's t-test. Scale bar 100 µm.

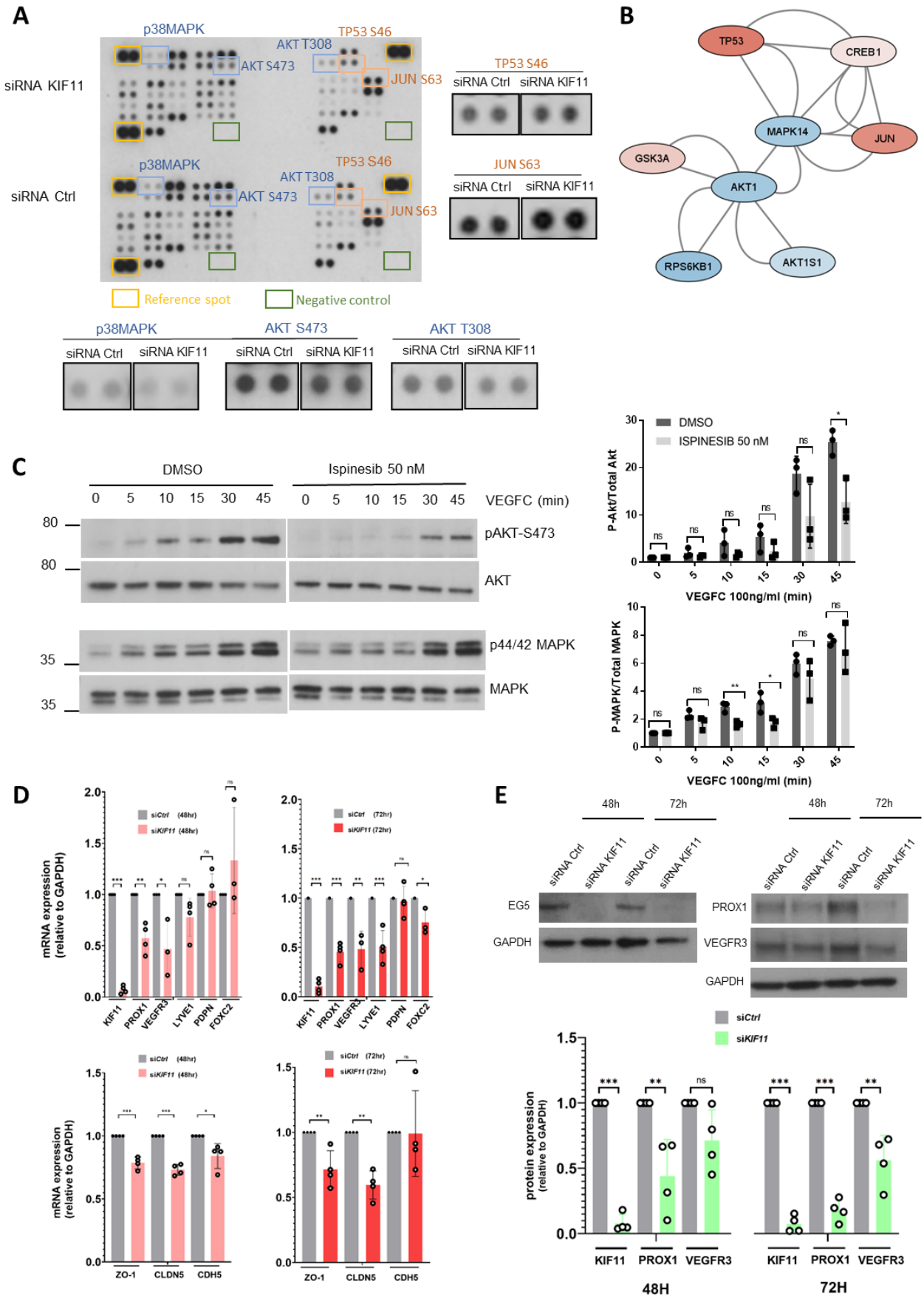
A
p38MAPK
AKT T308
TP53 S46
AKT S473
JUN S63
siRNA KIF11
siRNA Ctrl
TP53 S46
siRNA Ctrl siRNA KIF11
JUN S63
siRNA Ctrl siRNA KIF11
Reference spot
Negative control
p38MAPK
AKT S473
AKT T308
siRNA Ctrl siRNA KIF11
siRNA Ctrl siRNA KIF11
siRNA Ctrl siRNA KIF11
B
TP53
CREB1
MAPK14
JUN
GSK3A
AKT1
RPS6KB1
AKT1S1
C
DMSO
Ispinesib 50 nM
0 5 10 15 30 45
0 5 10 15 30 45
VEGFC (min)
80
pAKT-S473
80
AKT
35
p44/42 MAPK
35
MAPK
DMSO
ISPINESIB 50 nM
P-Akt/Total Akt
VEGFC 100ng/ml (min)
P-MAPK/Total MAPK
VEGFC 100ng/ml (min)
D
mRNA expression (relative to GAPDH)
siCtrl (48hr)
siKIF11 (48hr)
siCtrl (72hr)
siKIF11 (72hr)
KIF11 PROX1 VEGFR3 LYVE1 PDPN FOXC2
ZO-1 CLDN5 CDH5
E
48h 72h
siRNA Ctrl siRNA KIF11 siRNA Ctrl siRNA KIF11
EG5
GAPDH
PROX1
VEGFR3
GAPDH
siCtrl
siKIF11
protein expression (relative to GAPDH)
KIF11 PROX1 VEGFR3
48H
72H

Figure 8: *KIF11* deficiency alters MAPK and AKT signalling pathways and reduces expression of lymphatic cell identity and cell-cell junction markers. (A) Human Phospho-Kinase Array showing changes in phosphorylation levels of 43 kinases. Dots have been magnified for selected kinases with decreased (in blue) or increased (in red) phosphorylation. **(B)** Network pathway analysis using STRING and Cytoscape reveals known interactions and the directionallity of the phosphorylation change (blue, decreased and red, increased phosphorylation in siRNA *KIF11* treated cells). **(C)** Effect of Ispinesib treatment (50nM) on AKT and MAPK phosphorylation in LECs over time after stimulation with VEGFC (100ng/mL). DMSO (vehicle) treated cells as control. Phosphorylation was analysed with anti-pAKT S473 and anti-p44/42 MAPK Thr202/Tyr204 (upper panels) and levels of AKT and MAPK protein expression with anti-AKT and MAPK antibodies (lower panels). Molecular mass markers (in kDa) are indicated on the left. Blots are quantified (on the right). ns=not significant, *P<0.05, **P<0.01. Two-tailed unpaired Student's t-test. **(D)** *FLT4* (VEGFR3), *PROX1*, *PDPN, FOXC2*, *LYVE1, TJP1* (ZO-1)*, CLDN5 and CDH5* gene expression related to *GAPDH* in LECs treated with siRNA #6 *KIF11* for 48 and 72 hours analysed by qPCR (n=3-4 experiments). ns=not significant, *P<0.05, **P<0.01, ***P<0.001. Two-tailed unpaired Student's t-test. **(E)** Western blot analysis and quantification of PROX1 and VEGFR3 expression in LECs treated with siRNA *KIF11* for 48 and 72 hours. GAPDH was used as control. ns=not significant, **P<0.01, ***P<0.001. Two-tailed unpaired Student's t-test. (C-E) Bars represent mean relative expression ± SEM. (C and E) One representative image is shown from n=3-4 experiments.